Photon-echo interferometry to measure collision-induced optical phase shifts

A. M. Bacon, H. Z. Zhao, P. J. Laverty,* L. J. Wang, and J. E. Thomas
Physics Department, Duke University, Durham, North Carolina 27708-0305
(Received 8 June 1993)

We demonstrate a technique of photon-echo interferometry which provides extraordinary sensitivity for the measurement of the relative phase in the coherences for pairs of optical transitions. The method is applied to study collision-induced optical-coherence transfer between adjacent transitions in atomic samarium vapor.

PACS number(s): 34.40.+n, 42.50.Md

I. INTRODUCTION

We have developed a method of photon-echo interferometry which provides extraordinary sensitivity in studying collision-induced optical phase shifts. This technique has been applied to measure the relative phase shifts between two adjacent transitions due to collision-induced optical-coherence transfer. In this type of collision, the excited- and ground-state *amplitudes* are collisionally transferred between the adjacent transitions without complete destruction of the coherence. The echo-interferometry method employs backward stimulated photon echoes which are excited in two adjacent optical transitions in atomic samarium vapor. The backward echo fields from each of two transitions are emitted at the corresponding resonance frequencies, which are controllable with an adjustable magnetic field. When the difference frequency is appropriately tuned, the echo fields interfere destructively at the echo rephasing time, suppressing the echo intensity by a factor of 10^4. The suppression is strongly dependent on the relative phase of the two transitions, leading to great sensitivity in the measurement of collisionally induced relative phase changes between the adjacent transitions. This has enabled a study of very small collision-induced optical-coherence transfer rates, nearly two orders of magnitude smaller than measured previously for infrared transitions [1].

In the basic collision-induced coherence-transfer process, Fig. 1, optical coherence initially created on the a'-b' transition is collisionally transferred to the a-b transition and vice versa. Both the excited- and ground-state *amplitudes* of the active atom simultaneously change in this process, accompanied by a velocity change Δv. Formally, all theories of spectral line broadening contain contributions of collision-induced coherence transfer, the broadening rate comprising the total rate of loss of coherence by inelastic processes, velocity changes, or coherence transfer out of a given transition minus all rates of coherence arrival by transfer from neighboring velocity groups and neighboring degenerate transitions. Generally, these processes are most easily described by a quantum transport equation treatment [2–4]. To understand how collision-induced coherence transfer is related to the usual spectral line-broadening rate, it is convenient to consider the case where the spectral resolution is insufficient to resolve the Doppler frequency changes which accompany collision-induced velocity changes. Then, the evolution equations for the optical dipoles for two degenerate adjacent transitions of equal strength can be written in the form of rate equations, analogous to the case for a single two-level optical transition [5]. The equations for the optical dipole amplitudes for transition $i \leftarrow j$, $d_{ij}(t)$, take the form

$$\begin{aligned} \dot{d}_{ba}(t) &= -\gamma_T\, d_{ba}(t) + \gamma_v\, d_{ba}(t) + \gamma_c\, d_{b'a'}(t)\ , \\ \dot{d}_{b'a'}(t) &= -\gamma_T\, d_{b'a'}(t) + \gamma_v\, d_{b'a'}(t) + \gamma_c\, d_{ba}(t)\ , \end{aligned} \tag{1}$$

where γ_T is the total loss rate of optical coherence (optical dipoles) due to inelastic and elastic collisions and due to coherence transfer to the adjacent transition, γ_v is the arrival rate of coherence due to velocity changing collisions from adjacent velocity groups, and γ_c is the arrival rate of coherence from the adjacent transition. For transitions of equal strength, the evolution equation for the total dipole moment can be found by adding the evolution equations for d_{ba} and $d_{b'a'}$ to obtain

$$\frac{d}{dt}(d_{ba} + d_{b'a'})(t) = -\gamma_B\,(d_{ba} + d_{b'a'})(t)\ , \tag{2}$$

where γ_B corresponds to the usual line-broadening rate

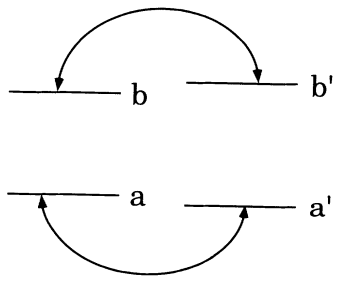

FIG. 1. Collision-induced coherence-transfer process. Excited- and ground-state *amplitudes* are collisionally transferred between adjacent transitions.

*Permanent address: Sparta, Inc., Huntsville, AL 35805.

in the impact approximation and is given by $\gamma_B = \gamma_T - \gamma_v - \gamma_c$. Hence, collision-induced coherence transfer from adjacent degenerate transitions reduces the effective line-broadening rate by canceling the coherence-transfer rate out of a given transition, which is inherent in the total loss rate γ_T.

In general, coherence transfer can occur between adjacent transitions in radio frequency, microwave, infrared, or optical transitions and has in principle been known for some time. However, the conditions under which collision-induced coherence transfer can occur are not well established, and have been studied experimentally in only a few instances. Processes of this type have been analyzed theoretically in some detail with neglect of the accompanying velocity changes [6, 7]. Previous experiments have studied collision-induced Zeeman coherence and microwave coherence rotational transfer (intramolecular) [8]. Studies of the Stark splitting dependence of the line-broadening rates [9] also involve collision-induced coherence transfer between transitions differing in magnetic quantum numbers. Finally, infrared coherence transfer in methyl fluoride has been studied by the method of tunable energy compensation [1]. This method, which tunably compensates a selected collision-induced Doppler shift with a Stark shift, determines the complete distribution of velocity changes accompanying collision-induced coherence transfer between adjacent transitions for which the magnetic quantum number differs by one.

The experiments described here are the first, to our knowledge, to study *optical*-coherence transfer [10], as opposed to infrared or microwave coherence transfer, which has been studied previously by a number of groups as described above. The samarium atomic system which we have explored provides an ideal system with just two adjacent optical transitions which are excited and probed in the experiments. Collision-induced optical-coherence transfer differs from coherence transfer between low frequency transitions in that the excited and ground states differ by an electronic energy, causing the ground- and excited-state collision potentials with perturbing gas species to be substantially different. In this case, one expects that optical phase disruption is likely to play an important role in the process. By contrast, the vibrational states excited in infrared experiments are very similar, and one expects little phase disruption. Hence it is not surprising that infrared experiments yield a large cross section for collision-induced coherence transfer [1], while it is unclear whether optical coherence survives collision-induced transfer at all. As described below, optical-coherence transfer does appear to make a substantial contribution to the phase shifts measured in our experiments. The rest of this paper is organized as follows. In the first section, the basic echo-interferometry method is described. Then a brief description of collision-induced coherence transfer and how it affects the echo intensity is given. Details of the derivations are relegated to Appendixes A and B. Finally, data from the experiments are presented and compared with calculations to investigate the contributions of collision-induced coherence transfer.

II. THEORY

A. Photon-echo interferometry

As described above, we have demonstrated a technique for photon-echo interferometry, whereby photon echoes generated on *independent* adjacent transitions in simple atoms are made to destructively interfere, suppressing the echo intensity by 10^4. The method is a form of polarization interference, as distinguished from quantum beats [11]. This technique serves as a sensitive probe of any perturbation which differentially affects the phase of the optical dipole moments of the adjacent transitions. Therefore the method is not limited to studies of collision-induced optical phase shifts as explored in the present work, where the method has been applied to investigate weak collision-induced optical-coherence transfer between the adjacent optical transitions.

The experiment, Fig. 2, employs two short, copropopagating optical pulses, separated by a time delay T, which excite the two adjacent transitions, $a \rightarrow b$ and $a' \rightarrow b'$, shown in Fig. 1. Just after the second pulse, a third *counterpropagating* pulse induces backward echo rephasing. For each transition, a backward echo is radiated at the atomic resonance frequency, causing temporal interference between the echo fields. By using a magnetic field to alter the relative frequency of the transitions, the interference can be adjusted.

The interference can be understood in more detail as follows. Just after the first pulse, at time $t = 0$, optical dipoles are excited which have a broad distibution of velocity v along the pump laser beam. In the atom frame, the optical dipole for the ith transition radiates at a frequency ω_{0i}. When the second pulse arrives at time T, the power absorbed by the dipole depends on the relative phase between the field of the second pulse and that of the dipole at time T. Due to the Doppler frequency shift, an atom moving at velocity v along the pump laser beam of frequency ω is affected by a laser frequency $\omega - kv$, where $k = 2\pi/\lambda$ is the optical wave vector. Hence the relative phase between the dipole created by the first pulse and the field of the second pulse is just

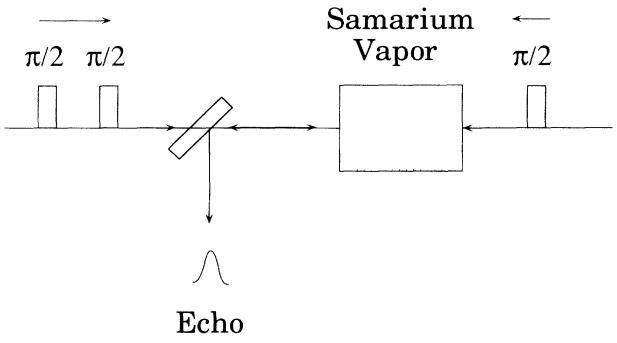

FIG. 2. Photon-echo interferometry. Two copropagating pulses followed by one counterpropagating pulse induce backward photon echoes radiated at the atomic resonance frequency. The radiation fields from adjacent transitions interfere constructively or destructively depending on the difference between the atomic resonance frequencies.

$(\omega - \omega_{0i} - kv)T$, which is velocity dependent. The power absorbed, and hence the population inversion, then takes the form of a grating or fringe in velocity space of the form $A(v)\cos[(\omega - \omega_{0i} - kv)T]$, where $A(v)$ is the shape of the velocity distribution for the population inversion as determined from the pulse shapes, and ω_{0i} is the optical transition frequency for each of the adjacent transitions: $i = 1, 2$, with $1 \equiv ba$ and $2 \equiv b'a'$. The third, counter-propagating pulse induces a macroscopic dipole moment in the sample of amplitude

$$d(t) \propto \sum_{i=1,2} \int dv\, A(v)\cos[(\omega - \omega_{0i} - kv)T] \times e^{-i(\omega_{0i} - kv)(t-T)}. \quad (3)$$

The part of Eq. (3) which rephases comes from the term containing $F(t-2T) \equiv \int dv\, A(v)\exp[ikv(t-2T)]$ and leads to a backward echo of intensity

$$I_{\text{echo}}(t) = \tfrac{1}{4}|F(t-2T)|^2 \left|e^{-i\omega_{01}t} + e^{-i\omega_{02}t}\right|^2. \quad (4)$$

Defining $\Delta\omega \equiv (\omega_{02} - \omega_{01})$, and $\tau \equiv t - 2T$, the time relative to the peak in the echo intensity at $t = 2T$, the echo intensity takes the simple form

$$I_{\text{echo}}(\tau) = |F(\tau)|^2 \cos^2\left[\frac{\Delta\omega}{2}(2T + \tau)\right]. \quad (5)$$

By adjusting the magnetic field strength so that $\Delta\omega T = \pi/2$, the echo intensity will be proportional to $\sin^2(\Delta\omega\tau/2)$ and is minimized at $\tau = 0$, i.e., at $t = 2T$, when the echo normally occurs. Experimental constructively and destructively interfering echoes are shown in Fig. 3. These are compared to the shape of the echo signals calculated in Appendix A as a function of τ for fixed $\Delta\omega$ which is given by Eq. (5) with $F(\tau) = 2\,g(\tau)$, according to Eq. (A55) where $g(\tau)$ is given by Eq. (A54). The calculated results are in good agreement with the measured signal shapes, including the small peaks on the left and right in Fig. 3.

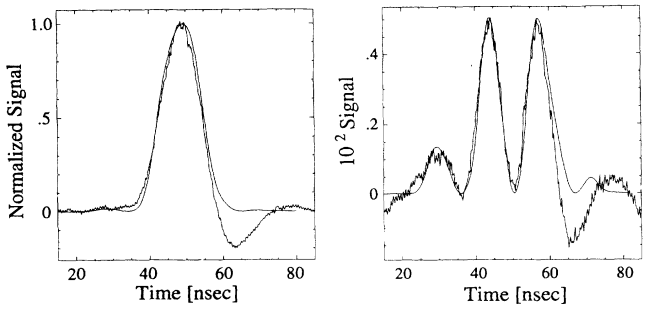

(a) (b)

FIG. 3. Photon-echo intensity in ^{152}Sm versus time in (a) zero magnetic field and (b) nonzero magnetic field (destructively interfered). The scale is normalized to unity for constructive interference. Note scale change of 10^{-2} for destructive interference. The null occurs at 50 nsec. The overshoot on the data is due to the high bandwidth amplifier. See Fig. 5 for level diagram.

B. Collision-induced optical-coherence transfer

The relative size of the two primary peaks in the destructively interfering echo signals is altered by foreign gas collisions. Exponential decay of the optical dipoles during the pump pulses and during the echo emission leads to a suppression of the right-hand peak, which occurs at later time than the left peak. In addition, optical *phase* shifts arise from two mechanisms: (i) collision-induced dipole destruction during the pump pulses which shortens the average evolution time for the optical dipoles and (ii) collision-induced optical-coherence transfer which alters the relative size of the two peaks in the destructively interfered echo signals.

To take into account the effects on the echo shape of collisions which *destroy* the optical dipole, it is convenient to use third order time-dependent perturbation theory in the density matrix equations, as described in detail in Appendix B. It is assumed in this part of the calculation that the Doppler shifts which accompany elastic collision-induced velocity changes are not resolvable for the short time scales and hence low spectral resolution used in the experiments. The neglect of velocity changes for elastic collisions permits a straightforward estimate of effects of collisions which destroy the optical dipoles *during* the pump pulses. The effects of optical-coherence transfer, which are neglected in Appendix B, are added in a separate calculation in Appendix A. In this case, the effects of large velocity changes which may accompany collision-induced coherence transfer at short range are included. Following Appendix B, it is assumed that the three pump pulses are Gaussian in shape with intensity $I(t) = \exp[-2(t - t_i)^2/(\tau_p^2)]$, where t_i is the center of the ith pulse, and τ_p is the pulse *field* $1/e$ width. The shape of the resulting echo intensity neglecting collisions is given by Eq. (5) where $F(\tau)$ is given by the convolution of the three Gaussian pulses so that

$$|F(\tau)|^2 = A_0\, e^{-\frac{2\tau^2}{3\tau_p^2}} \quad (6)$$

where $\tau = t - 2T$.

When collisions which destroy the optical dipoles are included, the amplitude A_0 is reduced by a factor $\exp[-4\gamma_B T]$, where T is the time between the first two pump pulses. Note that the third, backward propagating pulse is assumed coincident with the second forward propagating pump pulse. γ_B is the dipole destruction rate neglecting coherence transfer, and corresponds to the usual Lorentzian spectral line-broadening rate when the coherence transfer is included. In addition, Appendix B shows that the function given in Eq. (6) is modified by a factor $\exp[-8\gamma_B\tau/3]$, which takes into account collisions which destroy the optical dipole moment during the pump pulses, and during echo emission. Physically, the part of the echo signal appearing later in time arises from dipoles created earlier in time. This added evolution time leads to exponential decay which is dependent on the time τ relative to the echo peak. Hence the echo shape is the product of a Gaussian factor and an exponential, or equivalently, a shifted Gaussian with $\tau \to \tau + 2\gamma_B\tau_p^2$. Since terms of order $(\gamma_B\tau_p)^2 \ll 1$ in the exponential have

negligible pressure dependence for the short pulse durations used in the experiments, the echo shape can be represented equally well by shifting the argument in the cosine factor in Eq. (5) according to $\tau \rightarrow \tau - 2\gamma_B\tau_p^2$, and leaving the form of $|F(\tau)|^2$ as given by Eq. (6). For later data analysis, it will prove convenient to model the echo shape as a Gaussian factor multiplied by a cosine function with a pressure-dependent shift in the time argument. Dipole destroying collisions also contribute a relative phase shift to the echo fields which further modifies the argument of the cosine by a term proportional to $-\Delta\omega\gamma_B\tau_p^2$. Physically, this arises because the probability of a collision during a pump pulse is of order $\gamma_B\tau_p$. Hence, with a spread in dipole creation and observation times of order τ_p, the effective average evolution time of an optical dipole is shortened by $\Delta\tau \simeq \gamma_B\tau_p^2$. Thus, for dipoles oscillating at frequencies differing by $\Delta\omega$, a pressure-dependent phase shift $\simeq \Delta\omega\Delta\tau$ arises. Neglecting collision-induced coherence transfer, one obtains an echo shape of the form given by Eq. (7), with $I_c = 0$, i.e., no coherence transfer.

The calculation of the modification of the interfering echo signals due to collision-induced optical-coherence transfer is straightforward but tedious, and is carried out in Appendix A. Heuristically, coherence which is transferred from one transition to another adjacent transition at time t arrives with a time-dependent relative phase $\exp[\pm i\Delta\omega t + ik\Delta vt]$, where $\Delta\omega$ is the frequency difference between the optical dipoles of the adjacent transitions, created initially at $t = 0$, and Δv is the accompanying velocity change. The rate for coherence transfer with velocity change Δv is just $d\Delta v\, W_c(\Delta v)$, where W_c is the coherence-transfer kernel. The net fraction of coherence transferred between adjacent transitions during the time T between the first two pump pulses and the time T between the third pulse and the echo is determined by the velocity change integral and the time integral of the kernel with the time-dependent phase factor. The net result of collisional perturbation on the echo signal is obtained by modifying the result of the third order perturbation calculation, given by Eq. (B37), to include the effects of optical-coherence transfer, which is determined from Eq. (A55). The echo intensity then takes the form

$$I_{\text{echo}}(\tau) = A_0\, e^{-\frac{2\tau^2}{3\tau_p^2}} \left|\cos\left(\Delta\omega\{T_{\text{eff}} + \tfrac{2}{3}[\tau - c(p)]\}\right) + I_c\right|^2 , \tag{7}$$

where T_{eff} is the effective time separation between the first two pulses including effects of spontaneous emission during the pulses, and is pressure independent. $c(p)$ is the net pressure-dependent shift of the time argument due to collisions which destroy the optical dipoles as discussed above and is given by

$$c(p) = \left(3 - \frac{3}{2\pi}\right)\gamma_B'\tau_p^2 , \tag{8}$$

where γ_B' is the pressure-dependent part of the dipole destruction rate. Note that in Eq. (8), $2\gamma_B'\tau_p^2$ arises from the exponential decay of the signal during the echo emission, and the remainder arises from the relative phase shift of the two coherences due to dipole destroying collisions during the pump pulses and echo emission which effectively shorten the average dipole evolution time as described above. The effects of collision-induced optical-coherence transfer are contained in the I_c term of Eq. (7). In our experiments, the coherence-transfer rate is very small, so that $\gamma_c T \ll 1$, and the effects of collision-induced optical-coherence transfer need be carried out only to first order in $\gamma_c T$. From Appendix A, to lowest order in the coherence-transfer rate, I_c is given by Eq. (A45) as

$$I_c \equiv 2\,\text{Re}\left\{e^{-i\Delta\omega T}\int_0^T dt'\,\gamma_c(t')\right\}, \tag{9}$$

with

$$\gamma_c(t') \equiv \int d\Delta v\, W_c(\Delta v)\,\cos(k\Delta vt')\,e^{i\Delta\omega t'} . \tag{10}$$

$W_c(\Delta v)$ is the one dimensional coherence-transfer kernel which gives the rate of optical-coherence transfer between the adjacent transitions, accompanied by a velocity change Δv along the pump laser beam axis.

It is interesting to note that when $\Delta\omega = 0$, and the Doppler shifts accompanying collision-induced velocity changes are negligible (i.e., $k\Delta vT \ll 1$), then $I_c = 2\gamma_c T$, where γ_c is the integral of W_c over Δv. Then, according to the discussion above, the echo signal at time $2T$ is reduced by a factor $[\exp(-4\gamma_B T)]|1+2\gamma_c T|^2$. Since the neglect of coherence transfer in the calculation of the phase shift due to dipole destroying collisions is equivalent to taking $\gamma_B = \gamma_T - \gamma_v$ (i.e., $\gamma_c = 0$), we see that the net reduction of the echo signal is by a factor $\simeq \exp(-4\Gamma T)$, where $\Gamma = \gamma_T - \gamma_v - \gamma_c$, which is just the ordinary linebroadening rate as it should be. In our experiments, the product $\gamma_c T$ in the echo intensity is negligible for $\Delta\omega = 0$, but as shown below, for the destructively interfering echo signals, the contribution of coherence transfer to the observed asymmetry is quite significant.

When $\Delta\omega T_{\text{eff}} = \pi/2$, the echo intensity given by Eq. (7) for $|\Delta\omega\tau| \ll 1$ takes the form

$$I_{\text{echo}}(\tau) = A_0\, e^{-\frac{2\tau^2}{3\tau_p^2}}\,\frac{4(\Delta\omega)^2}{9}\,|\tau - c_0(p)|^2 , \tag{11}$$

where

$$c_0(p) \equiv c(p) + \frac{3}{2}\frac{I_c}{\Delta\omega} \tag{12}$$

includes the shift of the time due to both destructive collisions $c(p)$ and coherence transfer I_c.

When $\Delta\omega T = 3\pi/2$, the cosine term in Eq. (7) changes sign, so that Eq. (12) continues to be valid with $I_c \rightarrow -I_c$. As shown below [see Eq. (15)], I_c also changes sign in this case, so that the form of echo intensity given for the $\Delta\omega T = \pi/2$ case is valid also for the $3\pi/2$ case, except for a change in the magnitude of $\Delta\omega$.

Finally, it is important to note that the derivation of the results in Appendix A assumes that the pulses ex-

cite a broad velocity distribution of optical dipoles, such that the width of the distribution is large compared to the width of the collision-induced velocity changes. The full width at half maximum of the dipole velocity distribution is $\lambda[\mathcal{W}\ (\mathrm{Hz})]$, where $\lambda = 0.572\,\mu$ is the optical wavelength, and $\mathcal{W}$ is the excitation bandwidth, full width at half maximum. For a Gaussian pulse with a *field* $1/e$ width τ_p as assumed above, the corresponding bandwidth (full width at half maximum) is just $[\mathcal{W}\ (\mathrm{Hz})] = \sqrt{2\ln 2}/(\pi\tau_p) = 0.37/\tau_p$. From the fits to the experimental echo shapes (see below) using Eq. (11), $\tau_p = 5.5$ nsec, and $\mathcal{W} \simeq 67$ MHz. Hence the corresponding full width of the excited dipole distribution is 3800 cm/sec, large compared to the magnitude of the collision-induced velocity changes estimated from the experiments.

III. EXPERIMENT

In the experiments, Fig. 4, backward stimulated photon echoes are generated on the 572 nm $^7F_1 \rightarrow {}^7F_1$ transition in atomic samarium vapor, Fig. 5, for which the excited-state radiative lifetime is 152 nsec. Two copropagating, right-circularly polarized pump pulses of $\simeq 10$ nsec duration and $T = 50$ nsec separation are generated by acousto-optic modulation of stable cw dye laser light. These excite the $^7F_1$, $M = -1 \rightarrow {}^7F_1$, $M = 0$ transition and the adjacent $^7F_1$, $M = 0 \rightarrow M = 1$ transition which is of equal strength. Just after the second pump pulse, a third, *counterpropagating* right-circularly polarized pulse of 10 nsec duration induces backward echo rephasing on the same transitions. For each transition, a backward echo is radiated at the atomic resonance frequency, causing temporal interference between the echo fields which is adjustable using a magnetic field to alter the relative frequency of the transitions. Since both the forward pulse and backward echo are right-hand polarized with respect to the fixed $\hat{\mathbf{z}}$ axis, which is along the forward propagation direction, the right-hand polarized, backward propagating echo fields are phase shifted in passing back through the Soleil-Babinet compensator such that the echo is fully transmitted out of the escape window of the first glan prism.

Pulse generation is accomplished with a Stanford Research DG535 pulse generator. The echo intensity is detected with a Hamamatsu 1635 photomultiplier. This signal is amplified by a Sonoma 500 MHz bandwidth amplifier and sent to a boxcar averager for signal processing. The amplifier exhibits some overshoot, as on the right-hand side of Fig. 3, which does not appear when the signal is directly monitored with an oscilloscope. The pulse sequence is repeated at 17 kHz and the boxcar gate is temporally scanned by another output of the pulse generator to determine the echo shape. The integrated boxcar signal output is interfaced to a computer for subsequent data handling and analysis. To avoid drift of the laser frequency during the scan of the boxcar gate, the laser is frequency locked to a Lamb dip obtained with a separate reference cell containing samarium with no perturber gas. A tunable acousto-optic modulator is used to adjust the frequency offset to maximize the echo signals. An experiment to observe the pressure shift between the Lamb

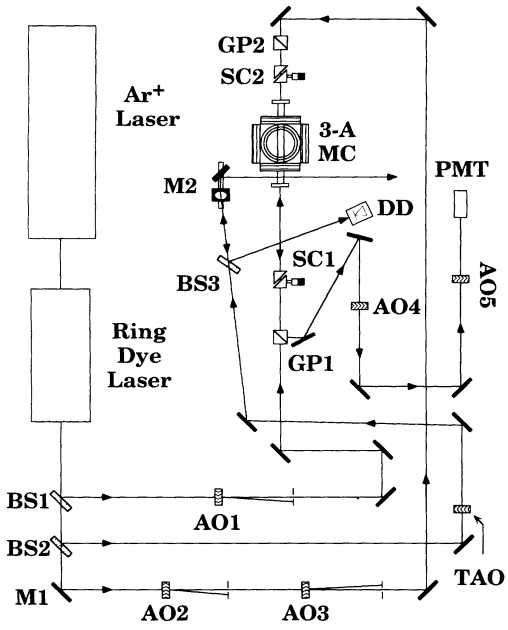

FIG. 4. Experimental setup. Beam splitter BS1 picks off a beam which is pulsed by an acousto-optic (AO) modulator (AO1) and right-circularly polarized by a glan prism (GP1) and Soleil-Babinet compensator (SC1) to create the two forward propagating pulses. Mirror M1 reflects a beam through AO1 and AO2 to create the third, backward-going pulse. (Two AO's are used to reduce the leakage light propagating toward the detector.) This beam is right-circularly polarized by GP2 and SC2. After passing through a cell surrounded by three axis magnetic coils (3-A MC), this beam is deflected out of the escape window of GP1 and sent through AO4 and AO5. These AO's are timed to block the third pulse and let through the echo. The echo signal is detected with a photomultiplier tube. Beam splitter BS2 picks off a beam that is sent by M2 to a vapor cell (not shown) on an elevated platform. The beam is passed through the cell, attenuated, and reflected back to create a Lamb dip in the absorption of the back reflected beam. The absorption signal monitored by a diode detector (DD) is used to lock the laser frequency. By changing the frequency of the Lamb dip beam with a tunable AO (TAO) the locked frequency of the laser can be adjusted.

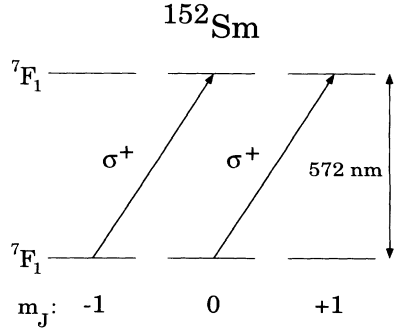

FIG. 5. Energy level diagram for ^{152}Sm.

dip obtained in the reference cell with no perturber vapor and a Lamb dip obtained in the echo cell with 600 mTorr argon perturber, the highest pressure used in the coherence-transfer experiments, shows that the shift is not measurable. Hence it is not necessary to equalize the perturber pressure in the echo and reference cells. Note that the two transitions utilized in the experiments are expected to have identical pressure shifts, so that the effect of any pressure shift between the reference and signal cells is of significance only due to the asymmetry of the echo signals induced by laser detuning. Since the excitation bandwidth is large, the effect of a very small pressure shift between the reference and signal cells is negligible.

Helmholtz coils are used to null the local magnetic fields for the echo measurements with $\Delta\omega = 0$, where the echo fields from the adjacent transitions constructively interfere. To set the magnetic fields for destructive interference of the echo fields, the $\hat{\mathbf{z}}$ component of the magnetic field is adjusted at zero perturber pressure to achieve a symmetric two peaked signal as shown in Fig. 3. The lowest magnetic field at which a symmetric, two peaked destructively interfering signal is obtained corresponds to the $\phi = \Delta\omega T = \pi/2$ case. Increasing the magnetic field until destructive interference occurs again at a higher magnetic field yields the $\phi = 3\pi/2$ case. For each magnetic field setting, the perturber pressure is gradually increased and the shapes of the echo signals are recorded at each pressure.

Figure 6 shows typical fits of Eq. (7) with $\Delta\omega = 0$ and Eq. (11) ($\Delta\omega T_{\text{eff}} = \pi/2$) to echo data taken at a pressure of 300 mTorr. A small peak which occurs on the left side of the data is ignored in the Gaussian approximation to the echo shape. With $T = 50$ nsec, five curves are fit for each pressure with $\phi = \Delta\omega T_{\text{eff}} = \pi/2$ to yield $c_0(p)$ as a function of pressure as shown in Fig. 7. The slope of the curve yields $c_0(p) = 3.23 \pm 0.25$ nsec/Torr. Fitting additional data, Fig. 8, which is obtained by changing *only the magnetic field* so that $\phi = \Delta\omega T_{\text{eff}} = 3\pi/2$, yields $c_0(p) = 2.87 \pm 0.30$ nsec/Torr.

Before analyzing the data in detail, we consider the function I_c of Eq. (9) in the short time or small velocity change limit, $k\Delta vT \ll 1$, and in the long time or large velocity change limit, $k\Delta vT \gg 1$. In the short time limit, the integrals over t' and Δv are readily carried out using $\int d\Delta v\, W_c(\Delta v) \equiv \gamma_c$, where γ_c is the total rate of collision-induced coherence transfer, which has been assumed real. Hence, for $k\Delta vT \ll 1$,

$$\frac{3}{2}\frac{I_c}{\Delta\omega} = \frac{3}{2}\,2\gamma_c\frac{\sin(\Delta\omega T)}{\Delta\omega^2}. \tag{13}$$

In the opposite limit, it is convenient to assume a Gaussian distribution for the velocity change Δv accompanying coherence-transfer collisions, so that the kernel takes the form

$$W_c(\Delta v) = \frac{\gamma_c}{\delta v\sqrt{\pi}}\, e^{-\left(\frac{\Delta v}{\delta v}\right)^2}. \tag{14}$$

In this case, the integration over Δv in Eq. (10) is readily carried out to obtain

$$I_c = 2\,\mathrm{Re}\left\{\gamma_c\, e^{-i\Delta\omega T}\int_0^T dt'\, e^{i\Delta\omega t'}\, e^{-\left(\frac{k\delta v t'}{2}\right)^2}\right\}. \tag{15}$$

In the long time, or large velocity change limit, $k\delta vT \gg 1$, one can take $T \to \infty$ in Eq. (15). For the destructively interfering echoes of interest here, $\Delta\omega T = \pi/2$ or $3\pi/2$, so that $\cos(\Delta\omega T) = 0$. In this case, I_c contains only the integral involving $\sin(\Delta\omega t')$. This can be evaluated in closed form if $\Delta\omega \ll k\Delta v/2$, so that the sine function can be expanded in a Taylor series. Keeping just the first two terms yields

$$\frac{3}{2}\frac{I_c}{\Delta\omega} \simeq \frac{3}{2}\sin(\Delta\omega T)\gamma_c\left(\frac{2}{k\delta v}\right)^2\left[1 - \frac{1}{6}\left(\frac{2\Delta\omega}{k\delta v}\right)^2\right]. \tag{16}$$

The experimental results show that difference in the shifts $c_0(p)$ is $\Delta c \equiv c_0(p)|_{\pi/2} - c_0(p)|_{3\pi/2} = 0.36 \pm 0.39$ nsec/Torr. Note that Δc is independent of the contributions due to exponential decay, $c(p)$, to the time shift $c_0(p)$ [see Eq. (12)], so that Δc depends only on the coherence-transfer contribution.

From the form of the short time, small velocity change limit of I_c given by Eq. (13), it is evident that the quantity $\frac{3}{2}\frac{I_c}{\Delta\omega}$ is reduced by a factor of 9 when $\Delta\omega T$ is increased from $\pi/2$ to $3\pi/2$. If it is assumed that the short

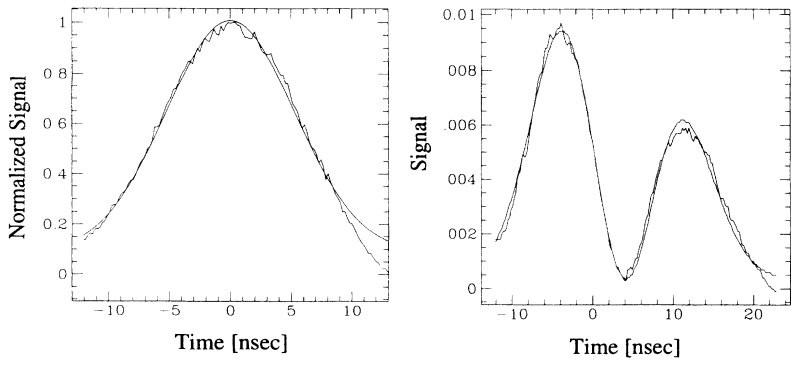

FIG. 6. Echo intensity versus time τ at 300 mTorr for (a) constructive interference ($\Delta\omega = 0$) and (b) destructive interference ($\Delta\omega T = \pi/2$). The scale is normalized to unity for the constructive interference peak. Note scale change of 10^{-2}.

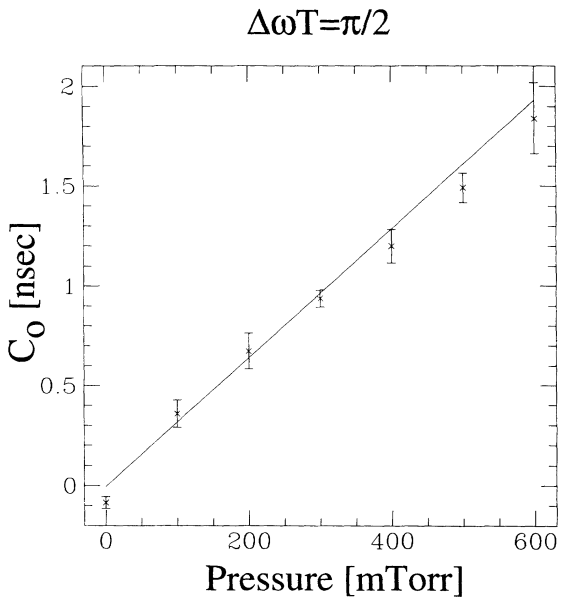

FIG. 7. Measured shift $c_0(p)$ as a function of pressure for $\Delta\omega T_{\text{eff}} = \pi/2$ showing linear variation. Slope: 3.23 ± 0.25 nsec/Torr.

time limit is valid, then

$$\frac{8}{3}\frac{\gamma_c}{(\Delta\omega_{\frac{\pi}{2}})^2} = \Delta c \ . \tag{17}$$

Using $\Delta\omega_{\frac{\pi}{2}} = \pi \times 10^7$ rad/sec, one obtains γ_c(Hz) =21.2 kHz/Torr. At 650 °C, the oven temperature used in the experiments, the relative speed for argon perturbers is $v_r = 7.8\times10^4$ cm/sec, and the density is $n_{\text{Ar}} = 1.12\times10^{16}$ /cm^3. This yields a coherence-transfer cross section σ_c from γ_c(rad/sec) $= n_{\text{Ar}} v_r \sigma_c$ of $\sigma_c \simeq 1.5$Å^2. This is the order of a hundred times smaller than the collision-induced coherence-transfer cross sections measured in Ref. [1].

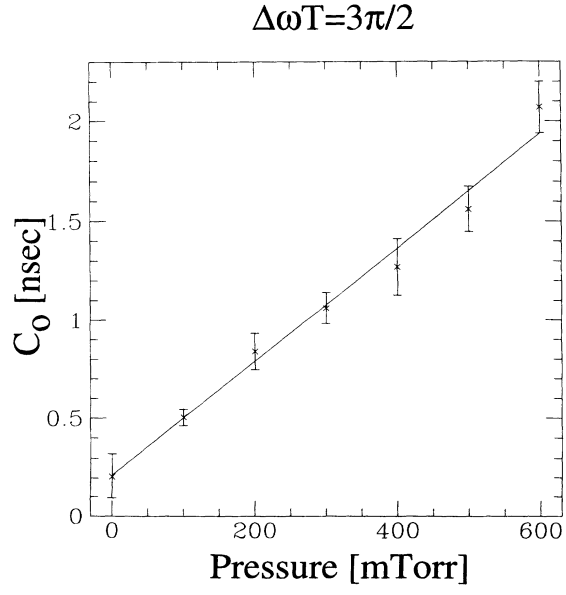

FIG. 8. Measured shift $c_0(p)$ as a function of pressure for $\Delta\omega T_{\text{eff}} = 3\pi/2$ showing linear variation. Slope: 2.87 ± 0.30 nsec/Torr.

The small size of the coherence-transfer cross section determined in the short time, small velocity change approximation shows that the photon-echo interferometry method is very sensitive. However, it is likely that such a small cross section would lead to large velocity changes, and hence violate the small velocity change approximation. Hence it is likely that the coherence-transfer rate is larger, and that the measured difference between the $\pi/2$ and $3\pi/2$ $c_0(p)$ slopes is reduced by two suppression effects due to large velocity changes as shown in Eq. (16). The suppression arises in the leading term of Eq. (16) which is smaller than that of Eq. (13) by a factor of order $\epsilon \equiv (2\Delta\omega/k\delta v)^2/2$, when $k\delta v > \Delta\omega$. Physically, the suppression of the effective coherence-transfer rate is due to the destruction of the population grating by collisional velocity changes larger than the period of the grating in velocity space. Such collisions cannot contribute to coherence transfer in atoms which contribute to the echo signal, and the effective transfer rate is reduced. In addition, the difference in slopes Δc between the $\pi/2$ and $3\pi/2$ data (Figs. 7 and 8) is in lowest order *independent* of $\Delta\omega$ in this case, so that only the second order terms in ϵ in Eq. (16) are dependent on $\Delta\omega$ if $k\delta v/2 \gg \Delta\omega$.

To analyze the data without the long or short time assumptions, we begin by writing the coherence-transfer contribution to the time shift $c_0(p)$ as

$$\frac{3}{2}\frac{I_c}{\Delta\omega_\phi} \equiv \frac{3}{2}\frac{2\gamma_c}{(\Delta\omega_\phi)^2}\int_0^\phi d\tau \exp^{-\left(\frac{k\delta v}{2\Delta\omega_\phi}\right)^2\tau^2} \sin\tau, \tag{18}$$

where $\phi \equiv \Delta\omega T$ is $\pi/2$ or $3\pi/2$.

The integral in Eq. (18) can be evaluated numerically for the cases $\phi = \pi/2$ and $3\pi/2$ as a function of the kernel width δv. For the experiments, $T = 50$ nsec, i.e., $\Delta\omega_\phi = \pi \times 10^7\,\text{sec}^{-1}$ for $\phi = \pi/2$, and $k = 2\pi/\lambda$, with $\lambda = 0.572\times10^{-4}$ cm. Holding $\Delta c = 0.36$ nsec/Torr, and using the results for the integrals appearing in Eq. (18), the value of γ_c can be plotted as a function of the kernel width δv, as shown in Fig. 9. This determines the possible choices for γ_c and δv which are consistent with the small difference between the measured slopes of the time shift, $c_0(p)$, for $\phi = \pi/2$ and $3\pi/2$.

Using the measured depolarization cross sections for the $^7F_1$ ground state of samarium with argon perturbers [12], an estimate of the magnitude of the coherence-transfer rate γ_c and hence of the coherence-transfer contribution to the time shifts $c_0(p)$ for the destructively interfering echo signals can be performed. The depolarization cross sections are given as $\sigma_0^{(1)} = 16.1$ Å^2 and $\sigma_0^{(2)} = 10.3$ Å^2. It is readily shown that the cross section for population transfer between adjacent magnetic sublevels is one-third of the rank two depolarization cross section, so that $\sigma_{\Delta M=1} = 3.4$ Å^2. This small cross section is due to the shielding of the ^7F core electrons by the $6s^2$ valence electrons in the ground state. For the excited state, one expects a much larger depolarization cross section, since the valence electrons are in a $6s6p$ configuration. The overlap of the excited-

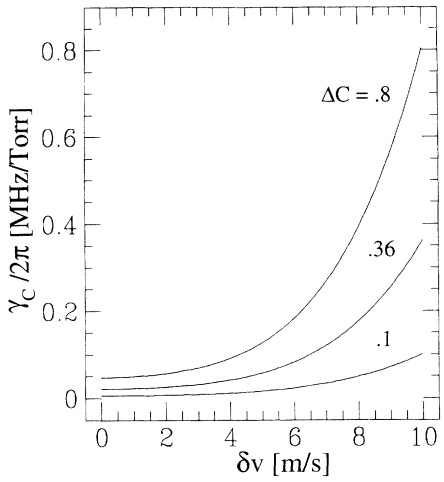

FIG. 9. Coherence transfer rate γ_c versus kernel width δv when the difference Δc of the slopes of Figs. 7 and 8 is constrained to equal 0.1 nsec/Torr, the experimental value 0.36 nsec/Torr, and to 0.8 nsec/Torr.

and ground-state scattering *amplitudes* determines the coherence-transfer cross section σ_c. Thus we assume that a reasonable value for the coherence-transfer cross section is $\sigma_c \simeq 10$ Å^2. At 650 °C, the oven temperature used in the experiments, the relative speed for argon perturbers is $v_r = 7.8 \times 10^4$ cm/sec, and the density is $n_{\mathrm{Ar}} = 1.12 \times 10^{16}$ /cm^3, yielding a coherence-transfer rate $\gamma_c(\mathrm{Hz}) = n_{\mathrm{Ar}} v_r \sigma_c/(2\pi) = 0.15$ MHz/Torr. At this value of the coherence-transfer rate, the width of the kernel consistent with the data must be $\delta v = 7.6$ m/sec according to Fig. 9. Note for comparison that the diffractive velocity change for a samarium atom scattering from a cross section $\sigma_c = \pi R^2$ is $\simeq 2\hbar/MR = 4.6$ m/sec, which is of comparable magnitude. Previous work on collision-induced infrared coherence transfer suggests that the corresponding kernels are of approximately diffractive width [1]. Using Eq. (18), one then obtains for the coherence-transfer contributions to the time shift

$$\frac{3}{2}\frac{I_c}{\Delta\omega_\phi}\Big|_{\phi=\pi/2} = 0.73\,\mathrm{nsec/Torr}\ , \tag{19}$$

$$\frac{3}{2}\frac{I_c}{\Delta\omega_\phi}\Big|_{\phi=3\pi/2} = 0.38\,\mathrm{nsec/Torr}\ . \tag{20}$$

Subtracting these values from the corresponding measured slopes $c_0(p)$ yields, according to Eq. (12), the value of $c(p)$, the time shift due to decay during the pulses, which should be independent of $\Delta\omega$. One obtains $3.23 - 0.73 = 2.5$ nsec/Torr for the $\pi/2$ data and $2.87 - 0.38 = 2.49$ nsec/Torr for the $3\pi/2$ data which are independent of magnetic field ($\Delta\omega$) as they should be for any choices of γ_c and δv related by Fig. 9.

To check that the value of $c(p) \simeq 2.5$ nsec/Torr is of reasonable magnitude, we calculate the approximate value expected on the basis of the simple perturbation calculation of Appendix B, and given by Eq. (8) above. By measuring the intensity decay of a two pulse echo versus time delay, we have determined that $\gamma'_B = 4.3$ MHz/Torr. Using Eq. (8) for $c(p)$, and the value of $(\tau_p)^2 = 30$ (nsec)^2 obtained from the fits to the echo shapes with Eq. (11), we find $c(p) = 2.0$ nsec/Torr, in reasonable agreement with the value 2.5 nsec/Torr estimated above. Note that larger values of γ_c and δv can be chosen according to Fig. 9 which increase the value of the coherence-transfer contribution to $c_0(p)$ and hence bring the remainder, $c(p)$, closer to 2 nsec/Torr. However, the small ground-state depolarization cross sections suggest that a much larger value of γ_c is not likely.

At present, our data and our calculation of $c(p)$ are too crude to extract reliable values of the coherence-transfer rate γ_c and of the kernel width δv directly from the measurements. However, the slope of the time shift $c_0(p)$ for the $3\pi/2$ data is approximately one standard deviation lower than the $\pi/2$ data, which is consistent with expectations that the coherence-transfer contribution decrease as $\Delta\omega$ is increased based on the predictions of Appendixes A and B.

IV. CONCLUSIONS

We have demonstrated a method of photon-echo interferometry which provides a sensitive means of measuring changes in the relative phase of adjacent independent optical transitions in simple atomic and molecular systems. By destructively interfering the echo signals from the adjacent transitions, suppression of the echo intensity by a factor of 10^4 has been obtained. The sensitivity is such that small collision-induced coherence-transfer rates, order of 10–100 kHz/Torr, can appreciably modify the symmetry of the destructively interfering echo signals. The method has enabled the first study of collision-induced *optical*-coherence transfer, as opposed to infrared or microwave coherence transfer, which occurs with rates more than a hundred times as large as in the present exeriments. The present experimental results indicate that collision-induced optical-coherence transfer probably causes approximately 25% of the total echo asymmetry (when $\Delta\omega T = \pi/2$). The remaining part of the asymmetry arises from collision-induced exponential decay of the optical dipoles during the pump and echo pulses, in the form of both amplitude and phase changes. Using the echo-interferometry method to make measurements for a transition with a longer radiative lifetime and a number of different input pulse delays T should enable a determination of the corresponding optical-coherence-transfer kernels. Finally, the echo-interferometry method should find general applications in precision measurement of the change in the relative phase of adjacent optical coherences due to external perturbations which differentially affect the transitions.

ACKNOWLEDGMENT

This research has been supported by the National Science Foundation through Grant No. PHY-89-22212.

APPENDIX A: BACKWARD STIMULATED ECHOES WITH OPTICAL-COHERENCE TRANSFER

As shown in the Introduction, backward stimulated echo fields arising from two adjacent transitions can in-

terfere constructively or destructively, depending on the difference between the resonance frequencies of the two transitions. In this section, the echo intensity is calculated, including the effects of collision-induced transfer of optical coherence between the adjacent transitions.

In the experiments, the $^7F_1 \rightarrow {}^7F_1$ transition in atomic samarium vapor is subjected to two near-resonant optical pulses of polarization $\hat{\mathbf{e}} = \hat{\sigma}_+$, propagating in the $+\hat{\mathbf{z}}$ direction, and separated by a time delay T. This creates velocity space gratings in the population inversions of the $^7F_1, M = -1 \rightarrow {}^7F_1, M = 0$ and adjacent $M = 0 \rightarrow M = 1$ transitions. A third pulse, also of polarization $\hat{\mathbf{e}}$, propagates in the $-\hat{\mathbf{z}}$ direction, and induces a backward stimulated echo. The field radiated by the sample following the third pulse can be written in the form

$$\vec{E} = \mathrm{Re}[\hat{\mathbf{e}}\mathcal{E}(z,t)\, e^{-ikz-i\omega_3 t}] \ . \tag{A1}$$

For a detector located outside the sample of length L, the slowly varying field amplitude is given by

$$\mathcal{E}(z,t) \simeq -2\pi ikL\,\mathcal{P}(t) \ , \tag{A2}$$

where it is assumed that the propagation delay L/c is negligible compared to the time scales of interest. The echo intensity is then given by

$$I_{\mathrm{echo}} = \frac{c}{8\pi}|\mathcal{E}(z,t)|^2 \ . \tag{A3}$$

The slowly varying envelope for the polarization, $\mathcal{P}$, is determined from

$$\vec{P} = \mathrm{Re}[e^{-ikz-i\omega_3 t}\mathcal{P}\vec{e}] = \mathrm{Tr}[\rho\vec{\mu}] \ , \tag{A4}$$

where ρ is the density operator and $\vec{\mu}$ is the dipole moment operator. For the two adjacent transitions of interest, labeled $a \rightarrow b$ and $a' \rightarrow b'$, the slowly varying polarization envelope can be written in the form

$$\mathcal{P} = \int dv\, [2\hat{\mathbf{e}}^*\cdot\vec{\mu}_{ab}\rho_{ba}(v,z,t)\, e^{ikz+i\omega_3 t}] + (a \leftrightarrow a'; b \leftrightarrow b'), \tag{A5}$$

where the second term is similar to the first term with the indicated substitutions.

The density matrix elements are calculated from the evolution equations for atoms moving with velocity v along the $\hat{\mathbf{z}}$ axis, including a one dimensional collision-integral term [2–4]

$$\left(\frac{\partial}{\partial t} + v\frac{\partial}{\partial z}\right)\rho(v,z,t) = -\frac{i}{\hbar}[H_0+U,\rho] + \left(\frac{d\rho}{dt}\right)^{\mathrm{coll}} . \tag{A6}$$

The interaction U with the laser fields takes the form

$$U = -\vec{\mu}\cdot\vec{E}(z,t). \tag{A7}$$

For the first two pulses, which are of equal intensity and of frequency ω, the field is given by

$$\vec{E}_p(z,t) = \hat{\mathbf{e}}\frac{\mathcal{E}_p(t)}{2}\, e^{ikz-i\omega t} + \mathrm{c.c.} \tag{A8}$$

The third pulse field takes the form

$$\vec{E}_3(z,t) = \hat{\mathbf{e}}\frac{\mathcal{E}_3(t)}{2}\, e^{-ikz-i\omega_3 t} + \mathrm{c.c.} \ , \tag{A9}$$

where it is assumed that the wave vectors of all fields are of approximately equal magnitude in determining the Doppler frequency shifts.

The optical coherences for the adjacent transitions, ρ_{ba} and $\rho_{b'a'}$, undergo velocity changing collisions with perturber vapor modeled by a one dimensional collision kernel $W_v(v-v')$ and collision-induced coherence transfer, modeled by the kernel $W_c(v-v')$. These kernels are the rates per unit velocity for a pure velocity change, $v-v'$, or for a coherence-transfer process to occur accompanied by a velocity change of the active atom. The coherence-transfer kernel W_c is dependent on an effective differential scattering cross section involving the overlap of the scattering amplitudes for excited- and ground-state changes, i.e., $f^*_{a\leftarrow a'}f_{b\leftarrow b'}$. The corresponding pure velocity changing kernel is dependent on the overlap of the elastic scattering amplitudes, $f^*_{a\leftarrow a}f_{b\leftarrow b}$. Since the transitions are of equal strength, we assume for simplicity that the kernels are real and further are symmetric functions of the velocity change, $\Delta v = v - v'$, for the small angle collisions of interest in this work.

Collision-integral terms for the coherences are then given by

$$\begin{aligned}\left(\frac{d\rho_{ba}}{dt}\right)^{\mathrm{coll}} &= -\gamma_T\rho_{ba}(v,z,t) \\ &\quad + \int dv'\, W_v(v-v')\,\rho_{ba}(v',z,t) \\ &\quad + \int dv'\, W_c(v-v')\,\rho_{b'a'}(v',z,t),\end{aligned} \tag{A10}$$

$$\left(\frac{d\rho_{b'a'}}{dt}\right)^{\mathrm{coll}} = (a \leftrightarrow a'; b \leftrightarrow b',),$$

where γ_T is the total loss rate of coherence from a given velocity group by elastic velocity changes, inelastic processes, and coherence transfer to other transitions. To simplify the calculations in this section, it is assumed that the laser pulse durations are sufficiently short that the effects of spontaneous emission and collisions *during* the pulses are negligible. This will allow an exact treatment of the shape of the interfering echo signal intensity to be given. In the next section, a perturbation treatment of the echo signals will be used to estimate the phase shifts caused by collisions during the pump pulses. During the time between pump pulses, it is assumed that the atomic density matrix evolves freely and undergoes collisions.

1. Evolution of the density matrix during the pump pulses

In order to calculate the change in the density matrix due to each of the three pump pulses, Fig. 10, it is convenient to determine the effect of a square pulse of length τ beginning at time t_0. With the neglect of spon-

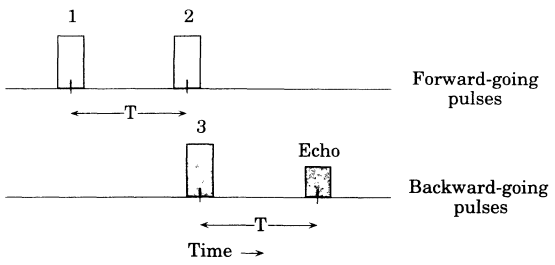

FIG. 10. Pump pulse sequence.

taneous emission and collisions, and using the rotating wave approximation, the evolution equations for the first two pump pulses (forward propagating) take the form

$$\left(\frac{\partial}{\partial t}+v\frac{\partial}{\partial z}\right)\rho_{ba}(v,z,t)$$

$$=-i\omega_{ba}\rho_{ba}(v,z,t)+i\frac{\vec{\mu}_{ba}\cdot\hat{\mathbf{e}}\mathcal{E}_p(t)}{2\hbar}e^{ikz-i\omega t}(\rho_{aa}-\rho_{bb})\ ,$$

$$\frac{\partial}{\partial t}\left[\rho_{bb}(v,t)-\rho_{aa}(v,t)\right]$$

$$=2i\frac{\vec{\mu}_{ba}\cdot\hat{\mathbf{e}}\mathcal{E}_p(t)}{2\hbar}e^{ikz-i\omega t}\rho_{ab}+\text{c.c.}\ ,$$

$$\frac{\partial}{\partial t}\left[\rho_{bb}(v,t)+\rho_{aa}(v,t)\right]=0\ . \tag{A11}$$

These equations are readily solved with the substitutions

$$\begin{aligned}\rho_{ba}(v,z,t)&=i(u-is)e^{ikz-i\omega t}\ ,\\ n&=\rho_{bb}-\rho_{aa}\ ,\end{aligned} \tag{A12}$$

$$\begin{aligned}\beta_p(t)&\equiv\frac{\vec{\mu}_{ba}\cdot\hat{\mathbf{e}}}{\hbar}\mathcal{E}_p(t)\ ,\\ \Delta'&=\omega-\omega_{ba}-kv\ ,\end{aligned}$$

where the functions $u(t)$ and $s(t)$ are real. With Eqs. (A11), the substitutions (A12) yield

$$\begin{aligned}\dot{n}&=2\beta_p(t)u\ ,\\ \dot{u}-\Delta' s&=-\frac{\beta_p(t)}{2}n\ ,\\ \dot{s}&=-\Delta' u\ .\end{aligned} \tag{A13}$$

These equations are readily solved for square pulses, where β_p is constant during each pulse, by differentiating the $\dot{u}$ equation to obtain

$$\ddot{u}+\beta'^2u=0\ , \tag{A14}$$

where

$$\beta'\equiv\sqrt{\Delta'^2+\beta_p^2}\ . \tag{A15}$$

Solving the second order equation for u subject to the initial conditions $u(t_0)$ and $\dot{u}(t_0)$ obtained from Eq. (A13) yields the solution for $u(t)$. The first order equations (A13) for n and s then are integrated to determine $n(t)$ and $s(t)$. The solutions are given in terms of the effective pulse area $\phi'\equiv\beta'\tau$ as

$$\begin{aligned}u(t_0+\tau)&=u(t_0)\cos\phi'+\left[\frac{\Delta'}{\beta'}s(t_0)-\frac{\beta_p}{2\beta'}n(t_0)\right]\sin\phi'\ ,\\ s(t_0+\tau)&=s(t_0)\left[\frac{\beta_p^2}{\beta'^2}+\frac{\Delta'^2}{\beta'^2}\cos\phi'\right]\\ &\quad-\frac{\Delta'}{\beta'}\sin\phi'\,u(t_0)+\frac{\Delta'\beta_p}{2\beta'^2}(1-\cos\phi')n(t_0)\ ,\end{aligned} \tag{A16}$$

$$\begin{aligned}n(t_0+\tau)&=n(t_0)\left[\frac{\Delta'^2}{\beta'^2}+\frac{\beta_p^2}{\beta'^2}\cos\phi'\right]\\ &\quad+\frac{2\beta_p}{\beta'}\sin\phi'\,u(t_0)+\frac{2\beta_p\Delta'}{\beta'^2}(1-\cos\phi')\,s(t_0)\ .\end{aligned}$$

The echo intensity is calculated by propagating the density matrix through each of the evolution regions shown in Fig. 10, beginning with the first pump pulse. For the first pump pulse, $t_0=0$ and $\tau=\tau_1$ in Eqs. (A16). Since $\rho_{ba}(0)=0$, $u(0)=0$ and $s(0)=0$. The initial population inversion is $n(0)=-\rho_{aa}(v)\equiv-N(v)$, where $N(v)$ is the population of a *single* ground-state M level. With the definition $\phi_1'\equiv\beta'\tau_1$, u, s, and n are determined after the first pulse as

$$\begin{aligned}u(\tau_1)&=+\frac{\beta_p}{2\beta'}\sin\phi_1'\,N(v)\ ,\\ s(\tau_1)&=-\frac{\Delta'\beta_p}{2\beta'^2}(1-\cos\phi_1')N(v)\ ,\\ n(\tau_1)&=-\left[\frac{\Delta'^2}{\beta'^2}+\frac{\beta_p^2}{\beta'^2}\cos\phi_1'\right]N(v)\ .\end{aligned} \tag{A17}$$

Using Eq. (A12), Eqs. (A17) yield the coherence at the end of the first pulse as

$$\rho_{ba}(v,z,\tau_1)=-A_1(a)\,N(v)\,e^{ikz-i\omega\tau_1}\ , \tag{A18}$$

where $A_1(a)$ determines the amplitude of the coherence created on the $a\rightarrow b$ transition by the first pulse, and is dependent on $\Delta'=\Delta'_a\equiv\omega-kv-\omega_{ba}$ according to

$$A_1(a)\equiv\frac{\Delta'\beta_p}{2\beta'^2}(1-\cos\phi_1')-i\frac{\beta_p}{2\beta'}\sin\phi_1'\ . \tag{A19}$$

$A_1(a')$ will denote the corresponding amplitude for the $a'\rightarrow b'$ transition, with $\omega_{ba}\rightarrow\omega_{b'a'}$, etc.

2. Free and collisional evolution of the coherence

In order to determine the coherences ρ_{ba} and $\rho_{b'a'}$ at the beginning of the second pulse, it is necessary to solve Eqs. (A6) with $U=0$ and the collision-integral terms given by Eqs. (A10). This is readily accomplished in the approximation that the amplitude of the polarization is a slowly varying function of velocity v compared to the kernels which are assumed to be narrow functions of the velocity change $\Delta v\equiv v-v'$. To proceed, the coherence is assumed to take the form

$$\rho_{ba}(v,z,t) = d_{ba}(v,t)\, e^{\pm ik[z-v(t-T_0-T_v)]}\, e^{-i\omega_{ba}(t-T_0)} \tag{A20}$$

and similarly for $\rho_{b'a'}$. The dependence of ρ_{ba} on $z - v(t-T_0)$ and $\omega_{ba}(t-T_0)$ automatically assures that in the absence of collisions, the free evolution equation is satisfied for the given initial conditions at time T_0 with time-independent $d_{ba}(v,t)$. Hence $d_{ba}(v,t)$ will be time dependent only due to collisional evolution. The time T_v is chosen to be the coefficient of $\pm kv$ in the phase of ρ_{ba} just after the pulse that creates the coherence at time T_0. With the rapid velocity dependence in the phase factored out, the amplitude $d_{ba}(v,t)$ will be a slowly varying function of velocity. The $\pm$ in the phase kz allows for forward or backward propagating pump pulses. The initial condition on the amplitude d_{ba} is determined from

$$d_{ba}(v,T_0) = \rho_{ba}(v,z,T_0)\, e^{\mp i[kz+kvT_v]} \,. \tag{A21}$$

With the density matrix equations (A6), and the collision terms given by Eqs. (A10), the ansatz given by Eq. (A20) yields

$$\dot{d}_{ba}(v,t) = -\gamma_T\, d_{ba}(v,t) + \int dv'\, W_v(v-v') e^{\pm ik(v-v')(t-T_0-T_v)}\, d_{ba}(v',t) \times \int dv'\, W_c(v-v')\, e^{\pm ik(v-v')(t-T_0-T_v)} e^{i\Delta\omega(t-T_0)}\, d_{b'a'}(v',t) \,, \tag{A22}$$

where $\Delta\omega \equiv \omega_{ba} - \omega_{b'a'}$ and $\dot{d}_{b'a'}(v,t)$ satisifies an equation of the same form with $a,b \to a',b'$ and $\Delta\omega \to -\Delta\omega$. Assuming that the widths of the kernels are narrow in velocity space compared to the widths of the amplitudes d_{ba} and $d_{b'a'}$, the amplitudes can be factored outside the velocity integrals and evaluated at $v' = v$. With the definition $\Delta v = v - v'$, Eq. (A22) then can be simplified to obtain

$$\dot{d}_{ba}(v,t) = -\gamma_v(t-T_0-T_v)\, d_{ba}(v,t) + e^{i\Delta\omega T_v}\, \gamma_c(t-T_0-T_v)\, d_{b'a'}(v,t) \,, \tag{A23}$$

where

$$\gamma_v(t') \equiv \gamma_T - \int d\Delta v\, W_v(\Delta v)\, \cos(k\Delta v t') \tag{A24}$$

and

$$\gamma_c(t') \equiv \int d\Delta v\, W_c(\Delta v) \cos(k\Delta v t')\, e^{i\Delta\omega t'} \,. \tag{A25}$$

$d_{b'a'}(v,t)$ obeys an equation of similar form with $a,b \to a',b'$, $\Delta\omega \to -\Delta\omega$, which implies $\gamma_c(t') \to \gamma_c^*(t')$. To isolate the effects of coherence-transfer collisions, it is convenient to transform away the $\gamma_v(t')$ term in Eq. (A23), using

$$d_{ba}(v,t) = D_{ba}(v,t)\, e^{-\int_{T_0}^{t} dt''\, \gamma_v(t''-T_0-T_v)} = D_{ba}(v,t)\, e^{-\int_{-T_v}^{t-T_0-T_v} dt'\, \gamma_v(t')} \tag{A26}$$

and similarly for $D_{b'a'}(v,t)$. With Eqs. (A21) and (A26), the initial condition on D_{ba} is given by

$$D_{ba}(v,T_0) = d_{ba}(v,T_0) = \rho_{ba}(v,z,T_0)\, e^{\mp i[kz+kvT_v]}. \tag{A27}$$

The amplitudes D_{ba} satisfy

$$\dot{D}_{ba}(v,t) = e^{i\Delta\omega T_v}\, \gamma_c(t-T_0-T_v)\, D_{b'a'}(v,t) \,, \tag{A28}$$

$$\dot{D}_{b'a'}(v,t) = e^{-i\Delta\omega T_v}\, \gamma_c^*(t-T_0-T_v)\, D_{ba}(v,t) \,.$$

Note that D_{ba} and $D_{b'a'}$ are constant in the absence of coherence-transfer collisions, i.e., for $\gamma_c \to 0$.

It is expected that over the time scales T of the transient signals, the product $\gamma_c T \ll 1$ for the present experiments. In this case, it is convenient to solve Eqs. (A28) to first order in $\gamma_c T$, yielding the result

$$\begin{aligned} D_{ba}(v,t) &\simeq D_{ba}(v,T_0) + D_{b'a'}(v,T_0)\, e^{i\Delta\omega T_v} \times \int_{T_0}^{t} dt''\, \gamma_c(t''-T_0-T_v) \\ &= D_{ba}(v,T_0) + D_{b'a'}(v,T_0)\, e^{i\Delta\omega T_v} \times \int_{-T_v}^{t-T_0-T_v} dt'\, \gamma_c(t') \,, \end{aligned} \tag{A29}$$

where $D_{b'a'}(v,t)$ is given by an equation of similar form with $a,b \to a',b'$, and $\Delta\omega \to -\Delta\omega$, which implies $\gamma_c \to \gamma_c^*$ according to Eq. (A25).

The coherence ρ_{ba} can be found for times between the end the first pulse, $T_0 = \tau_1$, and the beginning of the second pulse, t_2. Comparing Eqs. (A18) and (A20) shows that $T_v = 0$. Then, Eq. (A27) yields

$$D_{ba}(v,\tau_1) = -A_1(a)\, N(v)\, e^{-i\omega\tau_1} \tag{A30}$$

and similarly for $D_{b'a'}$ with $A_1(a) \to A_1(a')$. Using Eqs. (A29) and (A26) in Eq. (A20) yields the coherence at time t_2 as

$$\begin{aligned} \rho_{ba}(v,z,t_2) = &- N(v) \left[A_1(a) + A_1(a') \int_0^{t_2-\tau_1} dt'\, \gamma_c(t') \right] \\ &\times e^{-\int_0^{t_2-\tau_1} dt'\, \gamma_v(t')} \\ &\times e^{ik[z-v(t_2-\tau_1)]}\, e^{-i\omega_{ba}(t_2-\tau_1)}\, e^{-i\omega\tau_1} \,, \end{aligned} \tag{A31}$$

where $\rho_{b'a'}$ is given by a similar equation with $a,b \leftrightarrow a',b'$ and $\gamma_c \to \gamma_c^*$. In Eq. (A31), the exponential factor containing γ_v describes the destruction of the coherence due to inelastic processes and collision-induced Doppler dephasing, while the factor containing γ_c takes into account the arrival of coherence from the neighboring transition.

3. The stimulated echo polarization

To proceed with the calculation of the stimulated echo intensity, it is necessary to find the population inversion just after the second pulse. The population inversion takes the form of a velocity space grating from which the third pulse induces a backward stimulated echo. Using Eqs. (A16) with $t_0 = t_2$, and $\tau = \tau_2$, $\phi' = \phi'_2 = \beta'\tau'_2$, and $\vec{k} = k\hat{\mathbf{z}}$ (forward propagation) yields

$$n(t_2+\tau_2) = n(t_2)\left[\frac{\Delta'^2}{\beta'^2} + \frac{\beta_p^2}{\beta'^2}\cos\phi'_2\right] + \frac{2\beta_p}{\beta'}\sin\phi'_2\, u(t_2) + \frac{2\beta_p\Delta'}{\beta'^2}(1-\cos\phi'_2)\, s(t_2)\ . \tag{A32}$$

Equations (A12) can be inverted to determine $s(t_2)$ and $u(t_2)$ in terms of $\rho_{ba}(t_2)$ as

$$s(t_2) = \tfrac{1}{2}\, e^{-ikz+i\omega t_2}\,\rho_{ba}(t_2) + \text{c.c.}\ , \tag{A33}$$

$$u(t_2) = \frac{1}{2i}\, e^{-ikz+i\omega t_2}\,\rho_{ba}(t_2) - \text{c.c.}$$

The term in Eq. (A32) containing $n(t_2)$ does not contribute to stimulated echo formation, and will not be needed. We will be interested in the case where the third and second pulses are nearly coincident, so that the population inversion does not change in the time interval between these two pulses. When the third *backward propagating* pulse excites the population inversion, $n(t_3) \simeq n(t_2+\tau_2)$, the coherence which is created will contain a phase factor proportional to $\exp[+ikv(t-t_3-\tau_3)]$. From Eq. (A31), the coherence $\rho_{ba}(t_2) \propto \exp[-ikv(t_2-\tau_1)]$. In this case, the only terms in $n(t_2+\tau_2)$ which rephase come from the ρ_{ba} parts of $s(t_2)$ and $u(t_2)$ which give a net phase proportional to $\exp[+ikv(t-t_3-\tau_3-t_2+\tau_1)]$ which rephases when $t \simeq t_3+t_2+\tau_3-\tau_1$. Hence the c.c. terms in Eqs. (A33) can be ignored since they contribute negligibly when the velocity integration is carried out. Using Eqs. (A33) in Eq. (A32) yields the part of the population inversion which contributes to stimulated echo formation as

$$n^{(a)}_{\rm SE}(t_2+\tau_2) = 2\,A_2(a)\, e^{-ikz+i\omega t_2}\,\rho_{ba}(t_2)\ , \tag{A34}$$

where the dependence of $n^{(a)}_{\rm SE}$ on the second pulse is determined by $A_2(a)$, which is given by

$$A_2(a) \equiv \frac{\Delta'\beta_p}{2\beta'^2}(1-\cos\phi'_2) - i\frac{\beta_p}{2\beta'}\sin\phi'_2\ , \tag{A35}$$

analogous to Eq. (A19). $n^{(a')}_{\rm SE}(t_2+\tau_2)$ takes a similar form to Eq. (A34) with $a,b,\leftrightarrow a',b'$. With Eq. (A31) for $\rho_{ba}(t_2)$, the part of the population inversion which contributes to stimulated echo formation is given as

$$n^{(a)}_{\rm SE}(t_2+\tau_2) = -\,2\,N(v)\,A_2(a)\left[A_1(a) + A_1(a')\int_0^{t_2-\tau_1} dt'\gamma_c(t')\right] \times e^{-\int_0^{t_2-\tau_1} dt'\,\gamma_v(t')}\, e^{i(\omega-\omega_{ba}-kv)(t_2-\tau_1)}\ , \tag{A36}$$

with a similar equation for $n^{(a')}_{\rm SE}(t_2+\tau_2)$, where $a,b,\leftrightarrow a',b'$, implying $\gamma_c \to \gamma_c^*$.

As described above, the third and second pulses are taken to be nearly coincident, so that $n(t_3) \simeq n(t_2+\tau_2)$, where $n(t_2+\tau_2)$ is given by Eq. (A36). In this case, the coherence ρ_{ba} just after the third pulse can be determined from Eqs. (A12) and (A16) using $\vec{k} = -k\hat{\mathbf{z}}$, and $\omega = \omega_3$. The result, after retaining only the population inversion terms which lead to stimulated echo formation, takes the same form as Eq. (A18), with the population inversion $-N(v)$ replaced by $n^{(a)}_{\rm SE}(t_2+\tau_2)$ and $\tau_1 \to t_3+\tau_3$. Hence

$$\rho_{ba}(v,z,t_3+\tau_3) = A_3(a)\, n^{(a)}_{\rm SE}(t_2+\tau_2)\, e^{-ikz-i\omega_3(t_3+\tau_3)}\ , \tag{A37}$$

with

$$A_3(a) \equiv \frac{\Delta'_3\beta_3}{2\beta'^2_3}(1-\cos\phi'_3) - i\frac{\beta_3}{2\beta'_3}\sin\phi_3, \tag{A38}$$

where $\beta_3 = \vec{\mu}_{ba}\cdot\hat{\mathbf{e}}\mathcal{E}_3/\hbar$, $\Delta'_3 = \omega_3 - \omega_{ba} + kv$, $\beta'_3 = \sqrt{\Delta'^2_3+\beta_3^2}$, and $\phi'_3 = \beta'_3\tau_3$.

The last step in determining the echo polarization in the presence of coherence-transfer collisions is to find the polarization after the third pulse. According to Eqs. (A37) and (A36), the rephasing part of the polarization just after the third pulse will have a velocity-dependent phase factor $\exp[-ikv(t_2-\tau_1)]$. Comparing this with Eq. (A20) with $T_0 = t_3+\tau_3$ for a backward pulse $(-k)$ shows that $T_v = t_2-\tau_1$. Equation (A20) then yields the rephasing part of the polarization in the form

$$\rho_{ba}(v,z,t) = d_{ba}(v,t)\, e^{-ik[z-v(t-t_3-\tau_3-t_2+\tau_1)]} \times e^{-i\omega_{ba}(t-t_3-\tau_3)} \tag{A39}$$

with

$$d_{ba}(v,t) = D_{ba}(v,t)\, e^{-\int_{-t_2+\tau_1}^{t-t_3-\tau_3-t_2+\tau_1} dt'\,\gamma_v(t')}\ , \tag{A40}$$

where $D_{ba}(v,t)$ is given according to Eq. (A29). Equations (A27) and (A37) yield

$$D_{ba}(v,T_0=t_3+\tau_3)=\rho_{ba}(v,z,t_3+\tau_3)\,e^{i[kz+kv(t_2-\tau_1)]}$$
$$=-2\,N(v)\,A_3(a)\,A_2(a)\left[A_1(a)+A_1(a')\int_0^{t_2-\tau_1}dt'\gamma_c(t')\right]$$
$$\times\,e^{-\int_0^{t_2-\tau_1}dt'\,\gamma_v(t')}\,e^{i(\omega-\omega_{ba})(t_2-\tau_1)}\,e^{-i\omega_3(t_3+\tau_3)}. \tag{A41}$$

$D_{b'a'}(v,T_0=t_3+\tau_3)$ is given by a similar result with $a,b\leftrightarrow a',b'$ implying $\gamma_c\rightarrow\gamma_c^*$. Using Eq. (A29) in Eq. (A40) and keeping terms only to first order in γ_cT, where T is the time scale of the transient signals, yields with Eq. (A39) the rephasing part of the coherence as

$$\rho_{ba}(v,z,t)=-2\,N(v)\,e^{-2\int_0^{t_2-\tau_1}dt'\,\gamma_v(t')}\,e^{-i\omega_3(t_3+\tau_3)+i\omega(t_2-\tau_1)}e^{-ikz-i\omega_{ba}(t-t_3-\tau_3)}\,e^{ikv(t-t_3-\tau_3-t_2+\tau_1)}$$
$$\times\left\{e^{-i\omega_{ba}(t_2-\tau_1)}\,A_3(a)\,A_2(a)\left[A_1(a)+A_1(a')\int_0^{t_2-\tau_1}dt'\,\gamma_c(t')\right]\right.$$
$$\left.+e^{i\Delta\omega(t_2-\tau_1)}\,e^{-i\omega_{b'a'}(t_2-\tau_1)}\,A_3(a')\,A_2(a')\,A_1(a')\int_0^{t_2-\tau_1}dt'\,\gamma_c(-t')\right\}. \tag{A42}$$

$\rho_{b'a'}$ is given by a similar equation with $a,b\leftrightarrow a',b'$, $\Delta\omega\leftrightarrow-\Delta\omega$, implying $\gamma_c\leftrightarrow\gamma_c^*$. It is assumed in Eq. (A42) that the time integrals involving γ_v and γ_c do not vary significantly over a pulse duration, so that the time t can be approximated by the echo time and we take $t-(t_3+\tau_3+t_2-\tau_1)\rightarrow 0$ in the integration limits.

In Eq. (A42), the zeroth order term in γ_c yields the usual stimulated echo signal. The first term containing γ_c denotes coherence transfer from the a',b' transition to the a,b transition during the time between the first and second pulses, while the second term containing γ_c denotes coherence transfer from the a',b' transition to the a,b transition during the time between the third pulse and the echo rephasing time.

The form of the coherence ρ_{ba} can be greatly simplified in the approximation that the pulses excite a bandwidth large compared to the difference between the resonance frequencies of the two transitions, $\Delta\omega$. In this case, $A_1(a')=A_1(a)$, etc. It is convenient to define $T\equiv t_2-\tau_1$ and $\tau\equiv t-t_3-\tau_3-t_2+\tau_1$ with

$$\Delta\omega\equiv\omega_{ba}-\omega_{b'a'}\,,$$
$$\bar{\omega}\equiv\frac{\omega_{ba}+\omega_{b'a'}}{2}. \tag{A43}$$

Factoring out the phase $\exp[-i\omega_{b'a'}(t_2-\tau_1)]$ in Eq. (A42), the coherence takes the form

$$\rho_{ba}(v,z,t)=-2\,N(v)\,e^{-2\int_0^T dt'\,\gamma_v(t')}\,e^{-i\omega_3(t_3+\tau_3)+i\omega T}$$
$$\times e^{-ikz-i\bar{\omega}(2T+\tau)}\,e^{ikv\tau}A_3(a)\,A_2(a)\,A_1(a)$$
$$\times[e^{-i\Delta\omega(T+\frac{\tau}{2})}+e^{-i\frac{\Delta\omega\tau}{2}}\,I_c]\,, \tag{A44}$$

where

$$I_c\equiv 2\mathrm{Re}\left\{e^{-i\Delta\omega T}\int_0^T dt'\,\gamma_c(t')\right\}. \tag{A45}$$

In obtaining Eq. (A45), we have used the fact that $\gamma_c(-t')=\gamma_c^*(t')$ according to Eq. (A25) assuming that the kernel W_c is a real, symmetric function of the velocity change as described above. The echo field amplitude is given by Eq. (A2) using Eq. (A44) in Eq. (A5) for the polarization amplitude as

$$\mathcal{E}(z,t)=-2\pi ikL\,(-4\vec{\mu}_{ba}\cdot\hat{e})^*\,e^{-2\int_0^T dt'\,\gamma_v(t')}\,e^{i\omega_3(t-t_3-\tau_3)+i\omega T-i\bar{\omega}(2T+\tau)}$$
$$\times\int_{-\infty}^{\infty}dv\,e^{ikv\tau}\,N(v)\,A_3(a)\,A_2(a)\,A_1(a)\left\{2\cos\left[\Delta\omega\left(T+\frac{\tau}{2}\right)\right]+2\cos\left(\Delta\omega\frac{\tau}{2}\right)I_c\right\}. \tag{A46}$$

In Eq. (A46), we use $A_1(a')=A_1(a)$, etc., since the pulse bandwidth is assumed large compared to $\Delta\omega=\omega_{ba}-\omega_{b'a'}$ and note that $\Delta\omega\leftrightarrow-\Delta\omega$ when $a,b\leftrightarrow a',b'$. Since the echo amplitude will be nonzero only for τ comparable to a pulse duration (we use sub-Doppler excitation), one can take $\cos(\Delta\omega\tau/2)\simeq 1$ in the I_c term which is already first order in small quantities (γ_cT). This is consistent with the neglect of times of the order of pulse durations in the limits of the integrals involving γ_c and γ_v. However, we retain the dependence on τ in the leading term in the square brackets, since it contributes to first order in small quantities, $\Delta\omega\tau$.

For sub-Doppler excitation with counterpropagating pulses of frequencies ω and $\omega_3=\omega+\Delta$, the echo signal is maximized when

$$\omega=\bar{\omega}-\frac{\Delta}{2},$$
$$\omega_3=\bar{\omega}+\frac{\Delta}{2}. \tag{A47}$$

The initial ground-state population for *one* transition, $N(v)$, is given by

$$dv\,N(v)=dv\,N_0\frac{e^{-\frac{v^2}{u_0^2}}}{u_0\sqrt{\pi}}=N_0\frac{e^{-\left(\frac{kv}{ku_0}\right)^2}}{ku/\sqrt{\pi}}\frac{d(kv)}{\pi}\,, \tag{A48}$$

where $u_0=\sqrt{2k_BT_0/M}$ is the thermal speed.

We will assume that all pulses have the same amplitude so that the Rabi frequency β_p is the same for all pulses.

Using the substitution

$$\beta_p x = kv + \Delta/2 \tag{A49}$$

in the velocity integral of Eq. (A46), the echo field can be written in terms of the Doppler broadened absorption coefficient α for two degenerated transitions of equal strength as used in the experiments,

$$\alpha = 2\,\frac{4\pi k|\mu_{ba}\cdot\hat{\mathbf{e}}|^2}{\hbar(ku_0/\sqrt{\pi})}\,N_0. \tag{A50}$$

Neglecting terms of order $\Delta\omega/(2\beta_p)$ in the amplitudes $A_1(a)$, etc. and using the resonance conditions Eq. (A47), and the definition of x, Eq. (A49), one obtains

$$\begin{aligned} A_1(a) &= -i\,f^*(x,\phi_1)\ , \\ A_2(a) &= -i\,f^*(x,\phi_2)\ , \\ A_3(a) &= -i\,f(x,\phi_3)\ , \end{aligned} \tag{A51}$$

where

$$f(x,\phi) = \frac{\sin\left(\frac{\phi}{2}\sqrt{1+x^2}\right)}{\sqrt{1+x^2}}\left[\cos\left(\frac{\phi}{2}\sqrt{1+x^2}\right) + i\frac{x}{\sqrt{1+x^2}}\sin\left(\frac{\phi}{2}\sqrt{1+x^2}\right)\right]\ . \tag{A52}$$

Using these results, the echo field, Eq. (A46), takes the form

$$\mathcal{E}(z,t) = -\alpha L\,\mathcal{E}_p\,e^{-2\int_0^T dt'\,\gamma_v(t')}\,e^{i\omega_3(T+\tau)+i\omega T-i\bar{\omega}(2T+\tau)-i\frac{\Delta}{2}\tau}\,g(\tau)\left\{2\cos\left[\Delta\omega\left(T+\frac{\tau}{2}\right)\right]+2\,I_c\right\}\ , \tag{A53}$$

where $T = t_2 - \tau_1$ and the echo shape as a function of the time $\tau = t - t_3 - \tau_3 - t_2 + \tau_1$ is given by

$$g(\tau) = \frac{1}{\pi}\int_{-\infty}^{\infty} dx\,e^{i\beta_p\tau x}\,e^{-\left(\frac{\beta_p x-\Delta/2}{ku_0}\right)^2}\,f^*(x,\phi_1)\,f^*(x,\phi_2)\,f(x,\phi_3)\ . \tag{A54}$$

Note that in Eq. (A53) we have taken $\cos(\Delta\omega\tau/2)\to 1$ as described above.

With Eq. (A53) for the echo field at resonance, the echo intensity is given according to Eq. (A3) as

$$I_{\rm echo}(\tau) = (\alpha L)^2\,I_p\,e^{-4\,{\rm Re}\int_0^T dt'\,\gamma_v(t')}\,|2\,g(\tau)|^2\left|\cos\left[\Delta\omega\left(T+\frac{\tau}{2}\right)\right]+I_c\right|^2\ , \tag{A55}$$

where

$$I_p = \frac{c}{8\pi}|\mathcal{E}_p|^2 \tag{A56}$$

is the intensity of each of the square pump pulses which are assumed to be of equal amplitude. Note that the peak of the function $|2\,g(\tau)|^2$ is not at $\tau = 0$, but is shifted by a fraction of a pulse duration. This is due to the definition $\tau = t - t_3 - \tau_3 - t_2 + \tau_1$, which for equal pulse durations implies $t = t_3 + t_2$ at $\tau = 0$, which is the correct time for the echo peak only for pulses of negligible duration.

APPENDIX B: PHASE SHIFT DUE TO COLLISIONS DURING THE PUMP PULSES

The technique of photon-echo interferometry is sensitive to the relative phase between the macroscopic polarizations of the two adjacent transitions, which radiate interfering echo fields at different frequencies. As the pressure of perturber vapor is increased, the small probability of a dephasing collision *during* the pump pulses leads to a change in the relative phase of the interfering echo fields which cannot be neglected when compared to effects of collision-induced optical-coherence transfer. In order to treat this phase shift approximately, a perturbation theory calculation of the echo fields is carried out in this section which takes into account the effects of collisions which arise during the pump pulses. Such a calculation neglects the effects of the strong pump pulse fields on collision-induced Doppler dephasing, but takes into account dephasing collisions. The calculated phase shift then can be incorporated into the general result for the echo intensity, calculated in Appendix A. In addition, the perturbation calculation, which assumes Gaussian laser pulses, permits a closed form result for the echo intensity to be obtained, which explicitly displays the time at which the echo intensity peaks. By contrast, the result obtained in the preceding section for strong pulses does not rephase exactly at $\tau = 0$, since the time $T = t_2 - \tau_1$ is not the time between the pump pulse *centers*.

To begin, we approximate the density matrix equations (A6) in the low velocity resolution limit, where the effect of collisions is simply to introduce exponential decay rates [5]. The electric dipole interaction is assumed to be of the form

$$U = -\vec{\mu}\cdot\left[\hat{\mathbf{e}}\frac{E(z,t)}{2} + \text{c.c.}\right] \tag{B1}$$

so that the density matrix evolution equations in the rotating wave approximation are given by

$$\begin{aligned} \left(\frac{\partial}{\partial t}+v\frac{\partial}{\partial z}\right)\rho_{ba}(v,z,t) &= -(\gamma_{ba}+i\omega_{ba})\rho_{ba}(v,z,t) + i\frac{\vec{\mu}_{ba}\cdot\hat{\mathbf{e}}}{2\hbar}\,E(z,t)\,(\rho_{aa}-\rho_{bb})\ , \\ \left(\frac{\partial}{\partial t}+v\frac{\partial}{\partial z}\right)\rho_{bb}(v,z,t) &= -\gamma_b\,\rho_{bb}(v,z,t) - \left[i\frac{(\vec{\mu}_{ba}\cdot\hat{\mathbf{e}})^*}{2\hbar}\,E^*(z,t)\rho_{ba} + \text{c.c.}\right]\ , \\ \left(\frac{\partial}{\partial t}+v\frac{\partial}{\partial z}\right)\rho_{aa}(v,z,t) &= -\gamma_a\,\rho_{aa}(v,z,t) + \left[i\frac{(\vec{\mu}_{ba}\cdot\hat{\mathbf{e}})^*}{2\hbar}\,E^*(z,t)\rho_{ba} + \text{c.c.}\right]\ , \end{aligned} \tag{B2}$$

with a similar equation for $\rho_{b'a'}$, etc. In Eq. (B2), the field amplitude takes the form

$$E(z,t) = \mathcal{E}(z,t)\, e^{-i\omega t} \ , \tag{B3}$$

with

$$\mathcal{E}(z,t) = [\mathcal{E}_1(t) + \mathcal{E}_2(t)]\ e^{ikz} + \mathcal{E}_3(t)\, e^{-ikz} \ . \tag{B4}$$

For simplicity, it is assumed that all pulses are of equal frequency, ω. The fields $\mathcal{E}_i(t)$ represent the three pulses of Fig. 10, in the limit of small area pulses. It is convenient to make the substitution

$$\rho_{ba}(v,z,t) = \sigma_{ba}(v,z,t)\, e^{-i\omega t}. \tag{B5}$$

The density matrix equations then take the form

$$\begin{aligned}
&\left(\frac{\partial}{\partial t} + v\frac{\partial}{\partial z}\right)\sigma_{ba}(v,z,t) + (\gamma_{ba} - i\Delta_{ba})\sigma_{ba}(v,z,t) = i\frac{\vec{\mu}_{ba}\cdot\hat{\mathbf{e}}}{2\hbar}\,\mathcal{E}(z,t)\,(\rho_{aa} - \rho_{bb}) \\
&\left(\frac{\partial}{\partial t} + v\frac{\partial}{\partial z}\right)\rho_{bb}(v,z,t) + \gamma_b\,\rho_{bb}(v,z,t) = -i\frac{(\vec{\mu}_{ba}\cdot\hat{\mathbf{e}})^*}{2\hbar}\,\mathcal{E}^*(z,t)\sigma_{ba} + \text{c.c.} \\
&\left(\frac{\partial}{\partial t} + v\frac{\partial}{\partial z}\right)\rho_{aa}(v,z,t) + \gamma_a\,\rho_{aa}(v,z,t) = +i\frac{(\vec{\mu}_{ba}\cdot\hat{\mathbf{e}})^*}{2\hbar}\,\mathcal{E}^*(z,t)\sigma_{ba} + \text{c.c.}
\end{aligned} \tag{B6}$$

where the detuning $\Delta_{ba} = \omega - \omega_{ba}$. These equations are easily solved in perturbation theory using the Green's function, $g(z-z', t-t')$, which satisfies

$$\left[\left(\frac{\partial}{\partial t} + v\frac{\partial}{\partial z}\right) + (\gamma - i\Delta)\right]\, g(z-z', t-t') = \delta(z-z')\delta(t-t') \ . \tag{B7}$$

The Green's function is readily found by Fourier transformation where $\gamma > 0$ ensures that the solution is causal. The result is given by

$$g(z-z', t-t') = \Theta(t-t')\, e^{(\gamma - i\Delta)(t-t')}\, \delta\big(z - z' - v(t-t')\big) \ , \tag{B8}$$

where $\Theta(t-t')$ is the Heaviside step function.

With Eqs. (B7), (B4), and (B8), the σ_{ba} is obtained to first order in $\mathcal{E}$ for atoms initially in the ground state a, $\rho_{aa}^{(0)} \neq 0$ as

$$\sigma_{ba}^{(1)}(v,z,t) = i\frac{\vec{\mu}_{ba}\cdot\hat{\mathbf{e}}}{2\hbar}\rho_{aa}^{(0)}(v)\, e^{ikz}\int_{-\infty}^{t} dt_1'\, \mathcal{E}_1(t_1')\, e^{-(\gamma_{ba} - i\Delta_{ba} + ikv)(t-t_1')} \ , \tag{B9}$$

where the z' integration has been carried out in the Green's function solution, setting $z' = z - v(t-t_1')$. Using Eq. (B9) in Eqs. (B7) yields the population difference due to the interaction of the second and third pulses with the coherence created by the first pulse. The effect of the first pulse in second order does not contribute to the backward stimulated echo of interest here. With Eq. (B8) for the Green's function, one obtains

$$\begin{aligned}
\rho_{aa}^{(2)}(v,z,t) - \rho_{bb}^{(2)}(v,z,t) &= i\frac{(\vec{\mu}_{ba}\cdot\hat{\mathbf{e}})^*}{2\hbar}\int_{-\infty}^{t} dt_2'\left[e^{-\gamma_b(t-t_2')} + e^{-\gamma_a(t-t_2')}\right] \\
&\quad\times\left[\mathcal{E}_2^*(t_2')\, e^{-ik[z-v(t-t_2')]} + \mathcal{E}_3^*(t_2')\, e^{ik[z-v(t-t_2')]}\right] \\
&\quad\times\sigma_{ba}^{(1)}[v, z-v(t-t_2'), t_2'] + \text{c.c.} \\
&= -\left|\frac{\vec{\mu}_{ba}\cdot\hat{\mathbf{e}}}{2\hbar}\right|^2 \rho_{aa}^{(0)}(v)\int_{-\infty}^{t} dt_2'\int_{-\infty}^{t_2'} dt_1'\left[e^{-\gamma_b(t-t_2')} + e^{-\gamma_a(t-t_2')}\right] \\
&\quad\times e^{-(\gamma_{ba} - i\Delta_{ba} + ikv)(t_2'-t_1')} \\
&\quad\times\mathcal{E}_1(t_1')\left[\mathcal{E}_2^*(t_2') + \mathcal{E}_3^*(t_2')\, e^{2ik[z-v(t-t_2')]}\right] + \text{c.c.}
\end{aligned} \tag{B10}$$

The third order coherence due to the interaction of the last two pulses with the population inversion of Eq. (B10) is then obtained using Eqs. (B7) and (B8) as

$$\begin{aligned}
\sigma_{ba}^{(3)}(v,z,t) &= i\frac{\vec{\mu}_{ba}\cdot\hat{\mathbf{e}}}{2\hbar}\int_{-\infty}^{t} dt_3'\, e^{-(\gamma_{ba} - i\Delta_{ba})(t-t_3')}\left[\mathcal{E}_2(t_3')\, e^{ik[z-v(t-t_3')]} + \mathcal{E}_3(t_3')\, e^{-ik[z-v(t-t_3')]}\right] \\
&\quad\times\left[\rho_{aa}^{(2)}(v, z-v(t-t_3'), t_3') - \rho_{bb}^{(2)}(v, z-v(t-t_3'), t_3')\right] \ .
\end{aligned} \tag{B11}$$

In Eq. (B11), using Eq. (B10), there are two possible terms which radiate a backward propagating field. These are proportional to $\exp(-ikz)$, and arise from the $\mathcal{E}_3(t_3')\mathcal{E}_1(t_1')\mathcal{E}_2^*(t_2')$ term and from the $\mathcal{E}_2(t_3')\mathcal{E}_1^*(t_1')\mathcal{E}_3(t_2')$ term which comes from the complex conjugate part of Eq. (B10). The latter does not rephase, as is shown from the net velocity-dependent phase for that term which is given by $\exp\{ikv[(t-t_3') + (t_2'-t_1') + 2(t_3'-t_2')]\}$. Since $t_3' \geq t_2' \geq t_1'$, and $t \geq t_3'$, it is not possible for the velocity-dependent phase to vanish. For the former, the velocity-dependent phase is

proportional to $\exp\{kv[t-t_3'-(t_2'-t_1')]\}$ which rephases as a backward stimulated echo when $t \simeq t_3' + (t_2' - t_1')$. Hence the third order coherence which rephases as a backward stimulated echo is given by

$$\sigma_{ba}^{(3)}(v,z,t) = -i\frac{\vec{\mu}_{ba}\cdot\hat{\mathbf{e}}}{2\hbar}\left|\frac{\vec{\mu}_{ba}\cdot\hat{\mathbf{e}}}{2\hbar}\right|^2 e^{-ikz}\int_{-\infty}^{t}dt_3'\int_{-\infty}^{t_3'}dt_2'\int_{-\infty}^{t_2'}dt_1'\left[e^{-\gamma_b(t_3'-t_2')}+e^{-\gamma_a(t_3'-t_2')}\right]$$
$$\times e^{-(\gamma_{ba}-i\Delta_{ba})(t-t_3')}\,e^{-(\gamma_{ba}-i\Delta_{ba})(t_2'-t_1')}$$
$$\times e^{ikv[t-t_3'-(t_2'-t_1')]}\,\rho_{aa}^{(0)}(v)\,\mathcal{E}_1(t_1')\,\mathcal{E}_2^*(t_2')\,\mathcal{E}_3(t_3')\ . \tag{B12}$$

The slowly varying polarization envelope $\mathcal{P}$ is determined from Eq. (A5) with $\omega_3 = \omega$ and Eq. (B5) as

$$\mathcal{P} = \int dv\,\left[2\hat{\mathbf{e}}^*\cdot\vec{\mu}_{ab}\,\sigma_{ba}(v,z,t)\,e^{ikz}\right] + (a\leftrightarrow a';b\leftrightarrow b')\ . \tag{B13}$$

The velocity integral in Eq. (B13) can be carried out using Eq. (A48) for $\rho_{aa}^{(0)}(v) = N(v)$ in Eq. (B12). For simplicity, we assume that the pulse bandwidth is small compared to the Doppler width so that

$$dv\,\rho_{aa}^{(0)}(v) \simeq \frac{N_0}{ku_0/\sqrt{\pi}}\frac{d(kv)}{\pi}\ . \tag{B14}$$

According to Eq. (B12), the required velocity integral takes the form

$$\int_{-\infty}^{\infty}dv\,\rho_{aa}^{(0)}(v)\,e^{ikv[t-t_3'-(t_2'-t_1')]} \simeq 2\frac{N_0}{ku_0/\sqrt{\pi}}\delta(t-t_3'-(t_2'-t_1'))\ . \tag{B15}$$

With Eqs. (B12) and (B15), Eq. (B13) yields the polarization envelope as

$$\mathcal{P}(t) = -i\frac{\hbar}{2}\frac{N_0}{ku_0/\sqrt{\pi}}\left|\frac{\vec{\mu}_{ba}\cdot\hat{\mathbf{e}}}{\hbar}\right|^4\int_{-\infty}^{t}dt_3'\int_{-\infty}^{t_3'}dt_2'\int_{-\infty}^{t_2'}dt_1'\left[e^{-\gamma_b(t_3'-t_2')}+e^{-\gamma_a(t_3'-t_2')}\right]$$
$$\times\ e^{-(\gamma_{ba}-i\Delta_{ba})(t-t_3')}\,e^{-(\gamma_{ba}-i\Delta_{ba})(t_2'-t_1')}$$
$$\times\,\delta(t-t_3'-(t_2'-t_1'))\,\mathcal{E}_1(t_1')\,\mathcal{E}_2^*(t_2')\,\mathcal{E}_3(t_3') + (a,b\rightarrow a',b')\ . \tag{B16}$$

To evaluate Eq. (B16), we assume for simplicity that three Gaussian pulses of equal amplitude and duration are applied and that second and third pulses are nearly coincident. In this case,

$$\begin{aligned}\mathcal{E}_1(t_1') &= \mathcal{E}_p\,g(t_1')\ ,\\ \mathcal{E}_1(t_2') &= \mathcal{E}_p\,g(t_2'-T_{21})\ ,\\ \mathcal{E}_1(t_3') &= \mathcal{E}_p\,g(t_3'-T_{21})\ ,\end{aligned} \tag{B17}$$

where T_{21} is the time delay between the centers of the first and second pulses and

$$g(t') \equiv e^{-\frac{t'^2}{\tau_p^2}}\ . \tag{B18}$$

With identical Rabi frequencies for the two transitions defined by $\beta_p \equiv \vec{\mu}_{ba}\cdot\hat{\mathbf{e}}\mathcal{E}_p/\hbar$ the echo field radiated by the sample of length L is given by Eq. (A2) using Eq. (B16) as

$$\mathcal{E}(t) = -\frac{\alpha L}{2}\mathcal{E}_p\left(\frac{\beta_p}{2}\right)^2\int_{-\infty}^{t}dt_3'\int_{-\infty}^{t_3'}dt_2'\int_{-\infty}^{t_2'}dt_1'\left[e^{-\gamma_b(t_3'-t_2')}+e^{-\gamma_a(t_3'-t_2')}\right]$$
$$\times\ e^{-(\gamma_{ba}-i\Delta_{ba})(t-t_3')}\,e^{-(\gamma_{ba}-i\Delta_{ba})(t_2'-t_1')}$$
$$\times\delta(t-t_3'-(t_2'-t_1'))\,g(t_1')\,g(t_2'-T_{21})\,g(t_3'-T_{21})$$
$$+\ (a,b\rightarrow a',b')\ , \tag{B19}$$

where the Doppler broadened absorption coefficient α is given by Eq. (A50).

The form of this result can be simplified by means of the following substitutions:

$$\begin{aligned}&\tau_1 = t_2' - t_1 - T_{21}, \qquad t_2' \text{ const}, \qquad dt_1' = -d\tau_1\ ,\\ &\tau_2 = t_3' - t_2', \qquad t_3' \text{ const}, \qquad dt_2' = -d\tau_2\ .\end{aligned} \tag{B20}$$

The delta function appearing in Eq. (B19) then takes the form $\delta(t-t_3'-T_{21}-\tau_1)$, where $T_{21}+\tau_1 = t_2'-t_1' \geq 0$. In this case, the integral over t_3' is readily carried out yielding the echo field as

$$\mathcal{E}(t) = -\frac{\alpha L}{2}\mathcal{E}_p\left(\frac{\beta_p}{2}\right)^2 e^{-2\gamma_B T_{21}}\left[e^{2i\Delta_{ba}T_{21}}\,I_{ba}(\tau) + (a,b\rightarrow a',b')\right]\ , \tag{B21}$$

where $\tau \equiv t - 2T_{21}$, $\gamma_{ba} = \gamma_{b'a'} \equiv \gamma_B$ is the coherence destruction rate which is taken to be real, with any pressure shift (identical for both transitions) being incorporated into Δ_{ba}. The integral $I_{ba}(\tau)$ is given by

$$I_{ba}(\tau) \equiv \int_0^\infty d\tau_2 \left(e^{-\gamma_b \tau_2} + e^{-\gamma_a \tau_2}\right) \int_{-T_{21}}^\infty d\tau_1 \, e^{-2(\gamma_B - i\Delta_{ba})\tau_1} \times g(\tau - 2\tau_1 - \tau_2)\, g(\tau - \tau_1 - \tau_2)\, g(\tau - \tau_1). \tag{B22}$$

In Eq. (B22), the time delay T_{21} can be taken large compared to the pulse duration τ_p. In this case, since the last g function limits $\tau - \tau_1 \simeq \tau_p$, then the second and first g functions require $\tau_2 \simeq \tau_p$ and $\tau_1 \simeq \tau_p$ so that one can put $T_{21} \to \infty \gg \tau_p$ in the τ_1 integral. The τ_1 integral is readily carried out using the substitution $\tau_1' = \tau - \tau_1$ with $d\tau_1 = -d\tau_1'$ and completing the square in the exponent which arises from the product of the Gaussian factors to obtain

$$I_{ba}(\tau) = \sqrt{\frac{\pi}{6}}\, \tau_p \, e^{-\frac{\tau_p^2}{6}(\Delta_{ba} + i\gamma_B)^2} \, e^{-\frac{\tau^2}{3\tau_p^2} - \frac{4}{3}(\gamma_B - i\Delta_{ba})\tau} \, I_0 \, , \tag{B23}$$

where

$$I_0 \equiv \int_0^\infty d\tau_2 \left(e^{-\gamma_b \tau_2} + e^{-\gamma_a \tau_2}\right) e^{-\frac{\tau_2^2}{2\tau_p^2} + (\gamma_B - i\Delta_{ba})\tau_2} \, . \tag{B24}$$

Since our goal is to find the *phase* shift due to collisions during the pump pulses, a small change in the amplitude of the signal can be neglected by assuming that $\gamma_a \tau_p \ll 1$ and $\gamma_b \tau_p \ll 1$ for the real population loss rates. In this case, the exponentials involving the population decay rates in Eq. (B24) can be set equal to 1. With the definition $\beta \equiv (\Delta_{ba} + i\gamma_B)\tau_p \sqrt{2}$, the factor I_0 then takes the simple form

$$I_0 = 2\sqrt{2}\, \tau_p \int_0^\infty dx \, e^{-i\beta x} \, e^{-x^2} . \tag{B25}$$

We are interested in the limit $\beta \ll 1$, in Eq. (B25). In this case, up to order β^2, the integral I_0 is given by

$$\begin{aligned} I_0 &\simeq \sqrt{2\pi}\tau_p \left[1 - \frac{\beta^2}{4} - i\frac{\beta}{\sqrt{\pi}}\right] \\ &= \sqrt{2\pi}\tau_p \left[1 - \frac{i}{\sqrt{\pi}}(\Delta_{ba} + i\gamma_B)\tau_p\sqrt{2} \right. \\ &\qquad \left. - \frac{(\Delta_{ba} + i\gamma_B)^2}{4} 2\tau_p^2\right] \\ &\simeq \sqrt{2\pi}\tau_p \left[1 + \sqrt{\frac{2}{\pi}}\gamma_B\tau_p - i\sqrt{\frac{2}{\pi}}\Delta_{ba}\tau_p - i\gamma_B\Delta_{ba}\tau_p^2\right] . \end{aligned} \tag{B26}$$

In Eq. (B26), we retain terms of first and second order in small quantities in the imaginary part which contributes to the phase, while retaining only terms up to first order in the real part. The result for I_0 can be written in the form

$$I_0 = \sqrt{2\pi}\tau_p \, A \, e^{-i\varphi} \, , \tag{B27}$$

where $A = 1 + \sqrt{2/\pi}\,\gamma_B\tau_p$ is the magnitude of I_0, which is weakly pressure dependent through $\gamma_B\tau_p \ll 1$, and the phase φ is given by

$$\begin{aligned} \varphi &= \arctan\left(\frac{\sqrt{\frac{2}{\pi}}\Delta_{ba}\tau_p + \gamma_B\Delta_{ba}\tau_p^2}{1 + \sqrt{\frac{2}{\pi}}\gamma_B\tau_p}\right) \\ &\simeq \sqrt{\frac{2}{\pi}}\Delta_{ba}\tau_p + \left(1 - \frac{2}{\pi}\right)\gamma_B\Delta_{ba}\tau_p^2 + O(\epsilon^3) \, . \end{aligned} \tag{B28}$$

With Eqs. (B27) and (B28), Eq. (B23) takes the form

$$I_{ba}(\tau) = \frac{\pi}{\sqrt{3}}\tau_p^2 \left(1 + \sqrt{\frac{2}{\pi}}\gamma_B\tau_p\right) e^{-\frac{\tau^2}{3\tau_p^2} - \frac{4}{3}\gamma_B\tau} \times e^{i\Delta_{ba}\left[\frac{4}{3}\tau - \sqrt{\frac{2}{\pi}}\tau_p - \left(\frac{4}{3} - \frac{2}{\pi}\right)\gamma_B\tau_p^2\right]} \, , \tag{B29}$$

where real terms in the exponents of Eq. (B23) which are of second order in small quantities are neglected.

Note that in Eq. (B29) any pressure shift of the resonance frequency can be incorporated into Δ_{ba} as described above, and is the same for both transitions. With Eqs. (B29) and (B21) for the echo field, the echo intensity is given by Eq. (A3) as

$$I_{\text{echo}}(\tau) = A_0 \, e^{-\frac{2\tau^2}{3\tau_p^2} - \frac{8}{3}\gamma_B\tau} \cos^2\frac{\Delta\omega}{2}\left(2T_{21} + \frac{4}{3}\tau - \tau_0\right) \, , \tag{B30}$$

where we have used the definitions $\Delta_{ba} = \omega - \bar{\omega} - \Delta\omega/2$, and $\Delta_{b'a'} = \omega - \bar{\omega} + \Delta\omega/2$ with $\bar{\omega} = (\omega_{ba} + \omega_{b'a'})/2$ and $\Delta\omega = \omega_{ba} - \omega_{b'a'}$.

The amplitude A_0 is given by

$$A_0 = I_p \frac{4}{3}\left(1 + 2\sqrt{\frac{2}{\pi}}\gamma_B\tau_p\right)\left(\frac{\alpha L}{2}\right)^2 \left(\frac{\beta_p\tau_p\sqrt{\pi}}{2}\right)^4 \times e^{-4\gamma_B T_{21}} , \tag{B31}$$

with I_p the pump pulse intensity given by Eq. (A56), and

$$\tau_0 = \sqrt{\frac{2}{\pi}}\tau_p + \left(\frac{4}{3} - \frac{2}{\pi}\right)\gamma_B\tau_p^2 \, . \tag{B32}$$

Equation (B30) can be simplified by noting that the peak echo signal is shifted from $\tau = 0$ due to the exponential decay. With the definition $\tau \equiv \tau' - 2\gamma_B\tau_p^2$, and neglecting terms of order $(\gamma_B\tau_p)^2$ in the exponent, the echo intensity is given by

$$I_{\text{echo}}(\tau') = A_0 \, e^{-\frac{2\tau'^2}{3\tau_p^2}} \times \cos^2\frac{\Delta\omega}{2}\left(2T_{21} + \frac{4}{3}\tau' - \frac{8}{3}\gamma_B\tau_p^2 - \tau_0\right) . \tag{B33}$$

Using Eq. (B32) for τ_0, the time argument of the cosine function is proportional to $2T_{21} + 4\tau'/3 - \tau_0'$, where

$$\tau_0' \equiv \left(4 - \frac{2}{\pi}\right)\gamma_B \tau_p^2 + \sqrt{\frac{2}{\pi}}\tau_p \ . \tag{B34}$$

It is useful to define the line-broadening rate as $\gamma_B = \gamma_B' + \gamma_s/2$ where γ_s is the spontaneous decay rate of the excited state and γ_B' is the pressure broadening rate. In this case, the pressure-*independent* part of the time argument in the cosine of Eq. (B33) can be written

$$2T_{\text{eff}} \equiv 2T_{21} - \left(4 - \frac{2}{\pi}\right)\frac{\gamma_s}{2}\tau_p^2 - \sqrt{\frac{2}{\pi}}\tau_p . \tag{B35}$$

The time argument of the cosine in Eq. (B33) then can be written as $2T_{\text{eff}} + \frac{4}{3}[\tau' - c(p)]$ where $c(p)$ is pressure dependent and given by

$$c(p) = \left(3 - \frac{3}{2\pi}\right)\gamma_B' \tau_p^2 \ , \tag{B36}$$

where we have factored out 4/3 from the pressure-dependent part of Eq. (B34).

The echo intensity is finally given by

$$I_{\text{echo}}(\tau') = A_0\, e^{-\frac{2\tau'^2}{3\tau_p^2}} \cos^2\left(\Delta\omega\{T_{\text{eff}} + \tfrac{2}{3}[\tau' - c(p)]\}\right) . \tag{B37}$$

[1] J. E. Thomas, J. M. Liang, and R. R. Dasari, Phys. Rev. A **42**, 1669 (1990); J. M. Liang, L. A. Spinelli, R. W. Quinn, R. R. Dasari, M. S. Feld, and J. E. Thomas, Phys. Rev. Lett. **55**, 2684 (1985).

[2] P. R. Berman, Phys. Rev. A **5**, 927 (1972).

[3] E. W. Smith, J. Cooper, W. R. Chappell, and T. Dillon, J. Quant. Spectrosc. Radiat. Transfer **11**, 1547 (1971); **11**, 1567 (1971).

[4] V. A. Alekseev, T. L. Andreeva, and I. I. Sobelman, Zh. Eksp. Teor. Fiz. **62**, 614 (1972) [Sov. Phys. JETP **35**, 325 (1972)].

[5] See P. R. Berman, T. W. Mossberg, and S. R. Hartmann, Phys. Rev. A **25**, 2550 (1982).

[6] S. Stenholm, J. Phys. B **10**, 761 (1977).

[7] W. E. Baylis, Phys. Rev. A **7**, 1190 (1973).

[8] See F. Rohart, B. Segard, and B. Marke, J. Phys. B **12**, 3891 (1979), and references therein.

[9] Ph. Brechignac, J. Chem. Phys. **76**, 3389 (1982).

[10] P. J. Laverty, A. M. Bacon, and J. E. Thomas, *QELS Technical Digest Series* (Optical Society of America, Washington, DC, 1991), Vol. 11, p. 24.

[11] See M. Koch, J. Feldman, G. von Plessen, E. O. Gobel, P. Thomas, and K. Kohler, Phys. Rev. Lett. **69**, 3631 (1993), and references therein.

[12] R. M. Lowe, D. S. Gough, R. J. McLean, and P. Hannaford, Phys. Rev. A **36**, 5490 (1987).

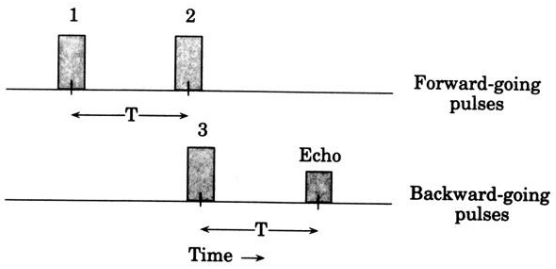

FIG. 10. Pump pulse sequence.